

The effect of different $\text{In}_2\text{O}_3(111)$ surface terminations on CO_2 adsorption

Sabrina M. Gericke,^{*,†,ⓐ} Minttu M. Kauppinen,^{*,‡,ⓐ} Margareta Wagner,[¶] Michele Riva,[¶] Giada Franceschi,[¶] Alvaro Posada-Borbón,[‡] Lisa Rämisch,[†] Sebastian Pfaff,[†] Erik Rheinfrank,[¶] Alexander M. Imre,[¶] Alexei B. Preobrajenski,[§] Stephan Appelfeller,[§] Sara Blomberg,^{||} Lindsay R. Merte,[⊥] Johan Zetterberg,[†] Ulrike Diebold,[¶] Henrik Grönbeck,[‡] and Edvin Lundgren[#]

[†]*Division of Combustion Physics, Lund University, 221 00 Lund, Sweden.*

[‡]*Department of Physics and Competence Centre for Catalysis, Chalmers University of Technology, 412 96 Göteborg, Sweden.*

[¶]*Institute of Applied Physics, TU Wien, 1040 Vienna, Austria.*

[§]*MAX IV Laboratory, Lund University, 221 00 Lund, Sweden.*

^{||}*Department of Chemical Engineering, Lund University, 221 00 Lund, Sweden.*

[⊥]*Department of Materials Science and Applied Mathematics, Malmö University, 205 06 Malmö, Sweden.*

[#]*Division of Synchrotron Radiation Research, Lund University, 221 00 Lund, Sweden.*

[ⓐ]*Contributed equally to this work*

E-mail: sabrina_maria.gericke@forbrf.lth.se; minttu.m.kauppinen@jyu.fi

Keywords

photoelectron spectroscopy, core-level shifts, heterogeneous catalysis, density functional theory, indiumoxide, CO₂ adsorption, methanol synthesis

Abstract

In₂O₃-based catalysts have shown high activity and selectivity for CO₂ hydrogenation to methanol, however the origin of the high performance of In₂O₃ is still unclear. To elucidate the initial steps of CO₂ hydrogenation over In₂O₃, we have combined X-ray Photoelectron Spectroscopy (XPS) and Density Functional Theory (DFT) calculations to study the adsorption of CO₂ on the In₂O₃(111) crystalline surface with different terminations, namely the stoichiometric, the reduced, and the hydroxylated surface, respectively. The combined approach confirms that the reduction of the surface results in the formation of In ad-atoms and that water dissociates on the surface at room temperature. A comparison of the experimental spectra and the computed core-level-shifts (using methanol and formic acid as benchmark molecules) suggests that CO₂ adsorbs as a carbonate on all surface terminations. We find that CO₂ adsorption is hindered by hydroxyl groups on the hydroxylated surface.

Introduction

The emission of greenhouse gases to the atmosphere has been identified as the origin of climate change.¹ CO₂ has been recognized as one of the main contributors to the greenhouse effect. One suggestion to mitigate its environmental impact is to capture CO₂ from the atmosphere, which introduces the challenge to contain the captured CO₂.² An appealing solution to this issue is the catalytical conversion of CO₂ into a more valuable fuel or platform chemicals.³ The hydrogenation of CO₂ using renewable H₂ from water splitting is one promising route for the catalytical conversion of CO₂ to useful oxygenates such as methanol CH₃OH, a key building block in the chemical industry and a renewable fuel.⁴ Methanol can be synthesized from CO₂ hydrogenation by thermal catalysis⁵, by electrocatalysis^{6,7} by photocatalysis.⁸ In thermal catalysis, Cu-ZnO-Al₂O₃ catalysts are commonly used for methanol synthesis. These Cu-ZnO-Al₂O₃ catalysts suffer, however, from deactivation, due to thermally induced sintering,⁹ agglomeration of ZnO species, and oxidation of metallic

Cu.¹⁰

In₂O₃-based catalysts have been suggested as an alternative to Cu–ZnO catalysts. Recent investigations of ZrO₂-supported In₂O₃ catalysts revealed high stability for CO₂ hydrogenation under industrial relevant conditions ($T = 473\text{--}573\text{ K}$, $p = 1.0\text{--}5.0\text{ MPa}$), as well as high activity and 100% selectivity for methanol synthesis.¹¹ The origin of the high performance of ZrO₂-supported In₂O₃ and the nature of the active sites of the catalysts have been the subject of intense investigations. Martin et al. proposed¹¹ that the high performance originates from the high concentration of oxygen vacancies in the In₂O₃. However, these surface oxygen vacancies do not exist on stoichiometric In₂O₃(111) under ultra high vacuum (UHV) conditions and could not be created by thermal reduction.¹² Additionally, kinetic modeling based on density-functional theory (DFT) suggests that oxygen vacancies are not crucial for the reaction but instead that a surface structure that allows for changes in the oxidation state of the In cations is needed.¹³ Furthermore, the quantification of oxygen vacancies is based on the appearance of an additional peak at higher binding energies in the O 1s X-ray Photoelectron Spectroscopy (XPS) spectra. However, previous and current calculations on the O 1s core-level shifts of In₂O₃ surfaces show that those peaks should be assigned to hydroxyl groups rather than oxygen vacancies.^{14,15}

Different atomic-scale reaction pathways have been suggested for CO₂-hydrogenation reactions. One is known as the reverse water–gas shift reaction (RWGS), which involves the dissociation of CO₂ and hydrogenation to methanol via a formyl (HCO) intermediate, whereas a more direct reaction pathway via the formation of formate (HCOO⁻) has also been discussed in the literature.⁴ The high selectivity of In₂O₃-based catalysts has been attributed to the suppression of the RWGS reaction,¹⁶ while the origin of RWGS suppression remains a subject of debate. Additionally, the effect of water on CO₂ hydrogenation has been discussed, and the inhibition of the CO₂ hydrogenation by water has been reported¹¹ although the underlying reason behind this effect remains unknown.

Fundamental investigations of a well-defined single crystalline In₂O₃ surface in a con-

trolled environment could advance the understanding of active sites and the effect of water on the CO₂ hydrogenation. The In₂O₃(111) surface is the thermodynamically most stable surface of In₂O₃ and has, moreover, been suggested to be active for CO₂ hydrogenation,¹⁷ making it of interest for fundamental and detailed investigations. In this paper, we apply a combined experimental synchrotron-based XPS measurements and computational DFT calculations of well-defined In₂O₃(111) surfaces prepared under pristine (i.e., UHV) conditions. Different surface terminations of In₂O₃(111) were investigated,^{12,18,19} namely the stoichiometric, the reduced, and the hydroxylated surface. Indium ad-atoms are identified via the In 3d core-level on the reduced surface, and OH-groups are identified via the O 1s core-level on the hydroxylated surface. The XPS fingerprints of these different surface terminations will facilitate the interpretation of future experiments performed at higher pressures. This work focuses on the adsorption of CO₂ on stoichiometric, reduced and hydroxylated surfaces under UHV conditions. We demonstrate that CO₂ forms carbonates with lattice oxygen atoms on all three surface terminations but the presence of OH groups limits CO₂ adsorption. Additionally, we investigated the adsorption of methanol and formic acid on the stoichiometric surface.

Experimental and Computational Methods

The In₂O₃(111) films of 200 nm thickness were grown on yttria-stabilized zirconia by pulsed-laser deposition in Vienna, as described in the literature.¹⁸ The films are single crystalline and exhibit atomically flat surfaces that can be prepared to exhibit different terminations following previously reported UHV treatments.^{12,19} The stoichiometric surface was prepared by gentle sputtering and subsequent annealing to 800 K in 2×10^{-6} mbar O₂ for 20 min and cooling in O₂. The reduced In₂O₃(111) surface was obtained by annealing the stoichiometric In₂O₃(111) in UHV at 720 K for 30 minutes. The hydroxylated surface was prepared by exposing the stoichiometric In₂O₃(111) to 1 Langmuir (1 L = 1.33×10^{-6} mbar s) of H₂O

at room temperature. Prior to the adsorption experiments with methanol and formic acid, the liquids were cleaned by a freeze–pump–thaw-cycle which was repeated three times. The stoichiometric surface was flashed to 475 K to desorb any OH-groups from the surface. Subsequently, the sample was cooled down to room temperature. Once the surface had reached room temperature, 1 Langmuir of methanol or formic acid were dosed, respectively, through a leak valve with a pressure of 5×10^{-9} mbar.

The XPS measurements were performed at the Surface Materials Science (SMS) branch of the FlexPES beamline at the MAX IV synchrotron.²⁰ This beamline is dedicated to high-resolution XPS and soft X-ray absorption measurements. The endstation is equipped with a Scienta DA-30 L analyzer and a preparation chamber with a low-energy electron diffraction (LEED) setup. We measured high-resolution XPS spectra of In $3d_{5/2}$ and O 1s with an excitation energy of 600 eV and C 1s at an energy of 400 eV to ensure high surface-sensitivity. All In $3d_{5/2}$ and the O 1s spectra were recorded with a pass energy of 20 eV and all C 1s with a pass energy of 50 eV. The spectra were recorded with an energy step size of 50 meV and the binding energy was calibrated on the valence band maximum (VBM) by setting it to 3.3 eV to compensate for band bending effects.²¹

We observed a minor potassium contamination on the sample, which accumulated on the surface when the sample was annealed. The contamination could be reduced by sputtering but not entirely removed, since it returned with annealing. The amount of potassium on the surface was estimated from the C 1s and K 2p XPS spectra. Based on the peak area of the spectra and the photoionization cross section, the potassium coverage is approximately 8% of the saturation methanol coverage which corresponds to 3 carbon atoms per unit cell. This means approximately 0.06 potassium atoms per unit cell or ≈ 0.05 at./nm². No other contaminants could be detected within the resolution limit of XPS. The ordering of the surface was ascertained by the presence of sharp LEED spots (see Fig. S1 in the SI).

The fitting of the core-level spectra was performed using the CasaXPS software package version 2.3.24.²² A Shirley background was used for the In $3d_{5/2}$ spectra and a linear back-

ground was used for the O 1s and the C 1s. The peak shapes that were used for the fitting are sum of a Gaussian and Lorentzian “SGL(p)”, and an asymmetric Lorentzian lineshape with tail damping “LA(α , β , m)”. Details on the fit functions can be found in the CasaXPS handbook.²²

The Vienna Ab initio Simulation Package (VASP, version 5.4.4)^{23–26} was used to perform DFT calculations with the Perdew-Burke-Ernzerhof (PBE)^{27,28} and the Heyd-Scuseria-Ernzerhof (HSE06)^{29–31} functionals. The PBE functional was employed for all structure relaxations and O 1s and In 3d core-level shifts, whereas HSE06 was used in the CO₂ adsorption calculations and the C 1s core-level spectra (see SI for details). The projector-augmented wave (PAW) method was used to describe the interaction between the core and the valence-electrons³² together with a plane-wave basis set with a 500 eV cutoff energy to expand the Kohn-Sham orbitals. The valence was chosen to be 1s¹, 2s²2p², 2s²2p⁴, and 4d¹⁰5s²5p¹ for H, C, O and In, respectively. The optimised bixbyite bulk structure for In₂O₃ was obtained from our earlier work.¹⁴ The In₂O₃(111) surface was modelled with a 1×1 surface cell of a thickness of five tri-layers (for surface termination studies and O 1s / In 3d core level shifts CLS) and three tri-layers (saturation coverage calculations and all hybrid calculations), with two or one bottom layers fixed at the optimised bulk positions, respectively. A 3×3×1 Monkhorst–Pack-mesh was used to sample the Brillouin zone for the PBE calculations, whereas the hybrid calculations were performed using the Gamma–point approximation. The core-level shift calculations included both initial and final state effects.^{33–35} The O 1s and In 3d shifts were computed as the difference in the energy of the system with a core hole on the atom of interest and the energy of the system with a core hole in a reference atom in the center of the slab, representing bulk In₂O₃. The C 1s shifts were computed as the difference in the energy of the system with a core hole on the atom of interest and the energy of the system with a core hole in the carbon atom of a methoxy (OCH₃) group placed in the same unit cell. To create the core holes, PAW potentials with one removed 3d (1s) electron were used for the In 3d (O 1s / C 1s) shifts. The charge neutrality of the computational cell

was maintained by employing a jellium background.^{36,37} Bader charges were calculated using the code developed by the Henkelman group.³⁸⁻⁴¹ Differential adsorption energies, ΔE_{diff} , of molecules on the surface were calculated as

$$\Delta E_{\text{diff}} = E_{\text{In}_2\text{O}_3+n\text{X}} - E_{\text{In}_2\text{O}_3+(n-1)\text{X}} - E_{\text{X}} \quad (1)$$

where $E_{\text{In}_2\text{O}_3+n\text{X}}$ and $E_{\text{In}_2\text{O}_3+(n-1)\text{X}}$ are the total energies of the $\text{In}_2\text{O}_3(111)$ surface slab with n adsorbed molecules and a slab with $n-1$ adsorbed molecules, respectively. E_{X} is the energy of the molecule in the gas phase, which were computed at Gamma point in a simulation box of 15 Å side length.

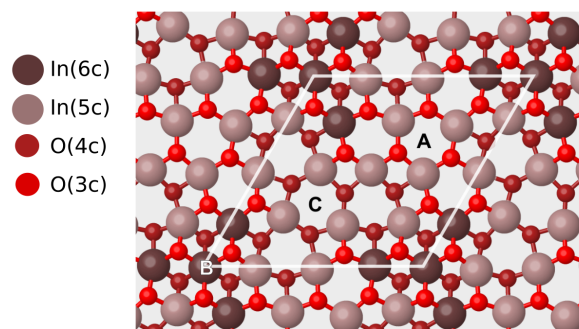
Results

In the following sections we present i) the characterisation of the different surface terminations of $\text{In}_2\text{O}_3(111)$ that will be used later to investigate CO_2 adsorption, ii) the adsorption of possible CO_2 reduction reaction intermediates (formic acid and methanol) on stoichiometric $\text{In}_2\text{O}_3(111)$, which we also use as benchmarks for C 1s CLS, and iii) the results for CO_2 adsorption on the stoichiometric, reduced, and hydroxylated surface terminations of $\text{In}_2\text{O}_3(111)$, respectively. In all sections, data from both experimental XPS and computational CLS are used to explore the structure and behavior of the $\text{In}_2\text{O}_3(111)$ surfaces.

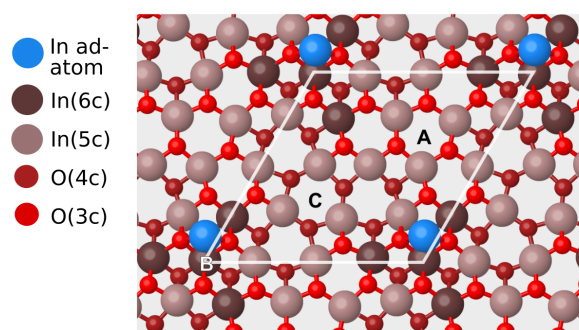
XPS fingerprints of the surface terminations of $\text{In}_2\text{O}_3(111)$

Figures 1(a), 1(b) and 1(c) show the atomic structures of the stoichiometric, reduced and hydroxylated $\text{In}_2\text{O}_3(111)$ surface terminations, respectively, as determined in our DFT calculations. The structures agree with previous studies of these surface terminations.^{12,18,19} The experimental preparation of the surface terminations is described in the methods section. Figure 2(a) and 2(b) show the XPS spectra of the O 1s and In 3d_{5/2} for the different surface terminations. The spectra were background subtracted and normalized to the intensity of

(a) stoichiometric $\text{In}_2\text{O}_3(111)$



(b) reduced $\text{In}_2\text{O}_3(111)$



(c) hydroxylated $\text{In}_2\text{O}_3(111)$

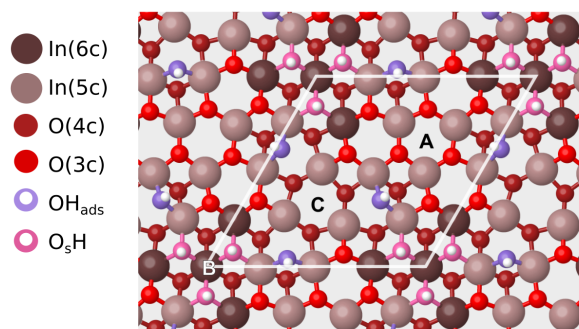


Figure 1: Top view of the first O–In–O trilayer of the surface terminations of (a) stoichiometric $\text{In}_2\text{O}_3(111)$, (b) reduced $\text{In}_2\text{O}_3(111)$ and (c) hydroxylated $\text{In}_2\text{O}_3(111)$. The six- and five-fold coordinated In atoms are shown in redbrown and beige, respectively, whereas O atoms occupying sites above and below the In layer are shown in bright and dark red, respectively. On the hydroxylated surface, the O atoms of the OH groups are colored pink for O atoms belonging to the oxide lattice (O_sH), and purple for the O atom originating from the dissociated water molecule (OH_{ads}). Indium ad-atoms are colored blue. Note that the configuration depicted is the two-fold coordinated ad-atom, which is iso-energetic with the structure depicted in ref. 13. The surface cell is indicated with white lines.

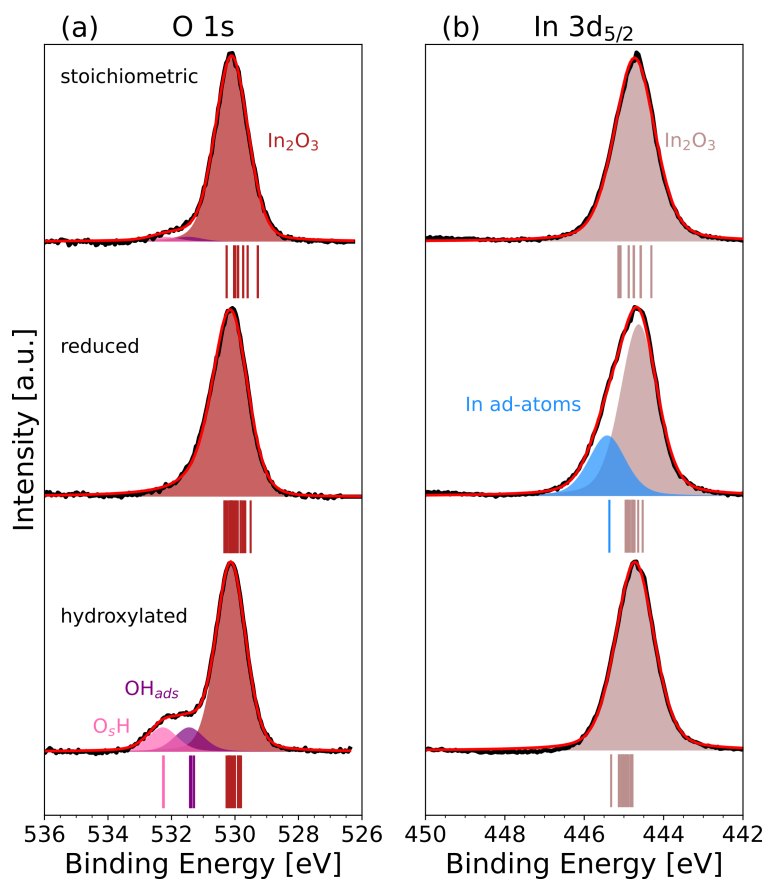


Figure 2: Panels (a) and (b) show the experimental O 1s and In 3d_{5/2} core-level spectra of the three different In₂O₃ surface terminations. The spectra were background subtracted and normalized to the intensity of the main peak. Calculated CLS are reported as vertical lines below experimental spectra, and the color coding is the same as in the corresponding structures (Figure 1).

the main peak. Details on line shapes and background functions are listed in Table S1 in the SI.

The spectra of stoichiometric $\text{In}_2\text{O}_3(111)$ show a main peak at 530.1 eV in the O 1s core-level, which corresponds to the $\text{In}_2\text{O}_3(111)$, and a small contribution of residual hydroxyl-groups at higher binding energies. In 3d_{5/2} core-level shows a single symmetric peak at 444.7 eV. Contributions from differently coordinated atoms, or a surface-core-level shift could not be resolved experimentally by varying the photon energy and the electron emission angle. The DFT calculations of the core-level shifts are presented below the XPS spectra. The different lines show the results for the different indium and oxygen atoms on the surface. The difference in atomic coordination results only in small shifts of the binding energies.

Reducing $\text{In}_2\text{O}_3(111)$ can, in principle, lead to either the formation of oxygen vacancies or indium ad-atoms. Previous STM studies on $\text{In}_2\text{O}_3(111)$ have reported that the thermal reduction of the $\text{In}_2\text{O}_3(111)$ surface results in the formation of an ordered array of indium ad-atoms with one ad-atom per unit.¹²

The experimental O 1s core-level spectrum of thermally reduced $\text{In}_2\text{O}_3(111)$ in Figure 2 shows a slight asymmetry towards higher binding energies. This observed asymmetry in the O 1s could result either from changes in the electronic structure of the In_2O_3 surface to a more metallic nature or from the adsorption of a small number of oxygen-containing molecules from the background gas such as small amounts of water. The In 3d_{5/2} shows a strong asymmetry towards higher binding energies, which originates from the formation of a new component in the XPS spectrum. The new component has a binding energy of 445.4 eV and the bulk In_2O_3 shifts by 0.1 eV to 444.6 eV due to band bending effects (see below). It is tempting to assign the component at higher binding energy to the indium ad-atoms previously observed for the reduced surface.¹² To validate this assignment, we calculated the relative binding energy shift of indium ad-atoms on the surface. We considered In ad-atoms placed at three different 3-fold symmetric sites on $\text{In}_2\text{O}_3(111)$ labelled A, B and C in Figure. 1 The relative stabilities, Bader charges and all In 3d CLS of the In ad-atoms on these sites

calculated with the PBE exchange-correlation functional are reported in Table S8 in the SI. Our calculated ad-atom stabilities are in complete agreement with previous DFT calculations performed with another implementation of the DFT equations.¹²

The most stable site for In ad-atoms is the B site, where the ad-atom can coordinate to three or two oxygen atoms. The structures are found to be nearly energetically degenerate (3 meV difference), suggesting that the ad-atom can move between the sites even at low temperatures. The In 3d core-level shifts were calculated for all In atoms in the first O–In–O trilayer for stoichiometric and reduced $\text{In}_2\text{O}_3(111)$. The In 3d shifts of the pristine surface cover a range of approximately 1 eV, with six (five)-coordinated In cations having negative (positive) shifts with respect to the bulk. The indium ad-atom on the reduced surface shows a positive shift compared to the other surface indium atoms. The experimentally observed shift of 0.8 eV for the reduced $\text{In}_2\text{O}_3(111)$ is very close to the 0.7 eV shift calculated for the ad-atom at the two-fold coordinated sites, indicating that In ad-atoms occupy the B site when the $\text{In}_2\text{O}_3(111)$ is reduced, which is in agreement with the previous STM and DFT study.¹²

We observed that the reduction of the surface causes band bending at the surface, which results in binding energy shifts of all core-levels. The effect of the band bending can be quantified from the position of the valence band maximum (VBM) by calibrating the spectra to the Fermi level of a gold foil mounted next to the sample at room temperature. The VBM is at 3.0 eV for the stoichiometric and hydroxylated surface, and at 3.2 eV for the reduced surface with In ad-atoms. A downwards band bending of 0.5 eV has previously been reported for $\text{In}_2\text{O}_3(001)$ ⁴² between the stoichiometric and the reduced $\text{In}_2\text{O}_3(001)$. The obtained band gap for $\text{In}_2\text{O}_3(111)$ is close to the band gap of single crystalline In_2O_3 which has been reported to be at 2.93 ± 0.15 eV and 3.02 ± 0.15 eV for the cubic bixbyite and rhombohedral polymorphs, respectively.⁴³

In the hydroxylation experiment with H_2O shown in Figure 2, a new component appears in the O 1s spectrum at higher binding energies relative to the lattice oxygen. The shoulder

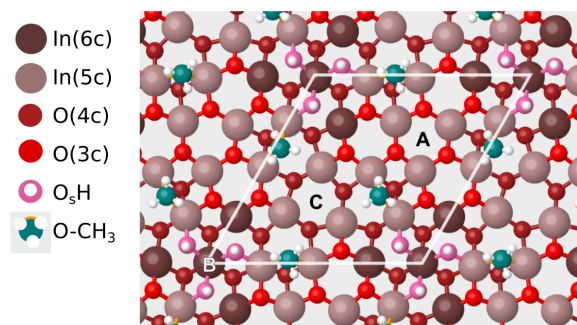
can be deconvoluted into two features with binding energies of 531.5 eV and 532.3 eV, which correspond to binding energy shifts of +1.3 eV and +2.1 eV, respectively.

The DFT calculations show that hydroxylation of the $\text{In}_2\text{O}_3(111)$ by water is energetically preferred. The adsorption energy of a single water molecule is -0.74 eV. Upon adsorption, the water molecule can easily dissociate at the B site with a low barrier of 0.05 eV¹³, and an exothermic reaction energy of -0.57 eV. Upon dissociation, two hydroxyl (OH) groups are formed on the surface, one is the OH fragment from water, which binds to the In cations on the surface OH_{ads} , and the other is formed as the proton from water binds to an oxygen atom on the $\text{In}_2\text{O}_3(111)$ surface O_sH . There are three equivalent sites close to the B site where water can adsorb dissociatively, and the effect of coverage on the adsorption energy is modest. Further adsorption of water takes place non-dissociatively at the C site with lower binding energies compared to the dissociative adsorption to B site. The O 1s and In 3d core-level shifts were calculated for the structure containing three dissociated water molecules (Figure 1(c)). The O 1s core-level shifts (Figure 2) show that the OH groups give rise to characteristic peaks at higher binding energies with respect to the other surface oxygen atoms. The average computed O 1s CLS is 2.2 eV for the three O_sH groups and 1.3 eV for the three OH_{ads} groups. The computed CLS for the two types of OH groups are in excellent agreement with the experimental XPS data (1.3 eV and 2.1 eV, respectively). The calculated O 1s CLS for molecularly adsorbed H_2O on the $\text{In}_2\text{O}_3(111)$ surface is over 3 eV with respect to the bulk¹⁴. The absence of a strongly shifted peak in the O 1s XPS supports the assessment that only dissociated water is present on the surface and is in agreement with the previous STM study of water on $\text{In}_2\text{O}_3(111)$, which showed that it is possible to achieve a coverage of three water molecules per $\text{In}_2\text{O}_3(111)$ unit cell at room temperature.^{19,44}

Methanol and formic acid on stoichiometric $\text{In}_2\text{O}_3(111)$

To study how the methanol product and possible reaction intermediate formic acid bind to the surface, their adsorption on stoichiometric $\text{In}_2\text{O}_3(111)$ was studied experimentally and

(a) Methanol on $\text{In}_2\text{O}_3(111)$



(b) Formic acid on $\text{In}_2\text{O}_3(111)$

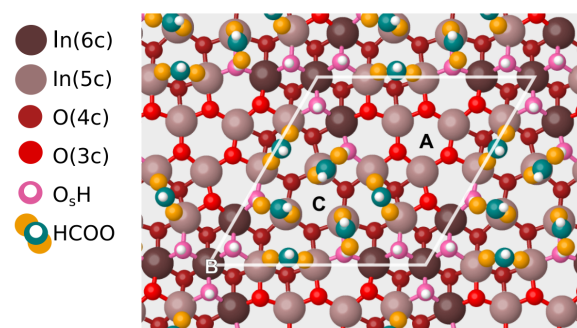


Figure 3: DFT-relaxed structures of (a) methanol and (b) formic acid on $\text{In}_2\text{O}_3(111)$. Carbon atoms of the HCOOH and MeOH molecules are colored teal, whereas their oxygen atoms are orange. In (a), the oxygen atom of the MeO^- is hidden by the carbon atom above it.

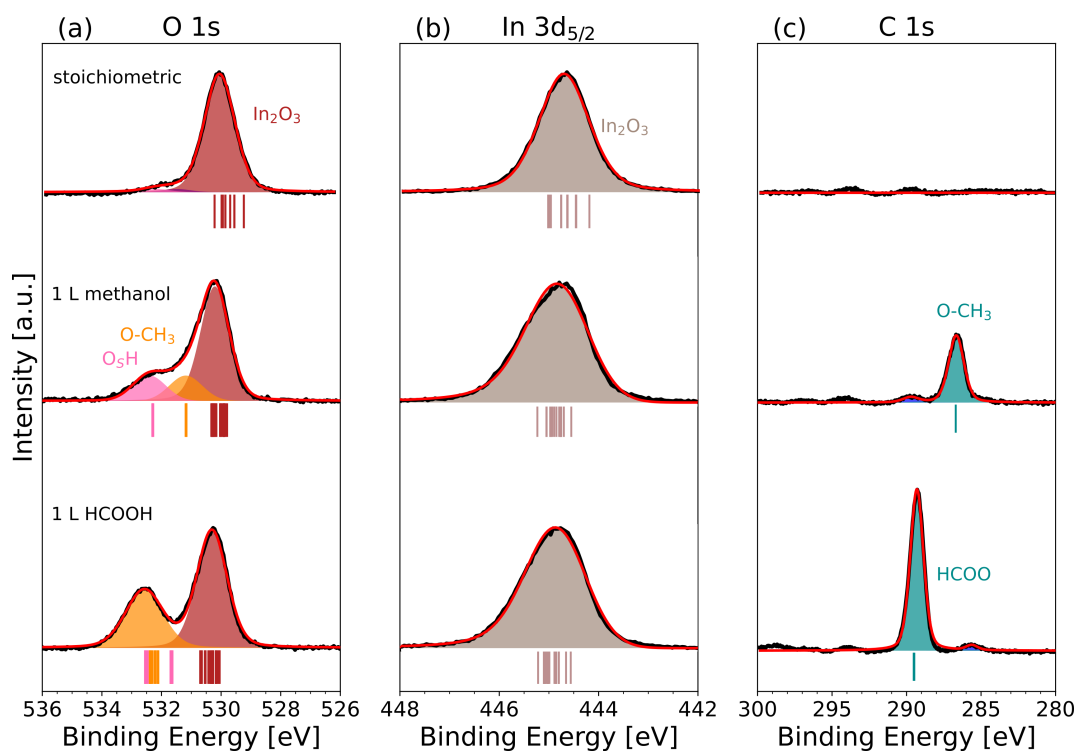


Figure 4: Panels (a), (b) and (c) show the experimental O 1s, In $3d_{5/2}$ and C 1s core-level spectra for the stoichiometric surface and methanol and formic acid adsorbed on $\text{In}_2\text{O}_3(111)$. Calculated CLS are indicated with vertical lines below experimental spectra. The color coding of the lines is the same as the coloring of atoms in the structural models (Figure 3).

computationally. Figure 3(a) shows the atomic configuration of methanol on stoichiometric $\text{In}_2\text{O}_3(111)$. Methanol was determined to preferably adsorb dissociatively on the $\text{In}_2\text{O}_3(111)$ forming H and O-CH₃ (with Bader charges of +0.63 and -0.70, respectively) pairs around the B site, preferring the same adsorption sites as dissociated water. The B site can accommodate three such pairs, which have very strong adsorption energies in the range of -1.2 to -1.0 eV. Achieving higher coverages requires the methanol to adsorb non-dissociatively around the C site, binding to an In cation through its oxygen atom. These methanol molecules have adsorption energies of only -0.5 to -0.4 eV, which suggest that only coverages of up to three methanol molecules per unit cell are achieved at room temperature.

The O 1s, In 3d_{5/2} and C 1s spectra of the methanol-covered surfaces are shown in Figures 4(a-c) along with the pristine $\text{In}_2\text{O}_3(111)$ for comparison. After methanol adsorption, the XPS spectra show two new peaks in the O 1s core-level at respective binding energies of 531.2 eV and 532.4 eV. These peaks can be assigned to the O-CH₃ fragment and the protonated oxygen atom at the B site O_sH. The shift between the peaks is calculated as 1.12 eV, which is in nice agreement with the experimental value of 1.2 eV. In the C 1s spectrum, the O-CH₃ groups result in a peak at 286.7 eV. The experimental In 3d_{5/2} spectrum shows an asymmetry to higher binding energy after the adsorption of methanol. This is qualitatively consistent with the calculated In 3d CLS: contributions from surface In atoms are found at slightly higher binding energies than for the pristine surface. The asymmetry originates from the superposition of the bulk signal (at lower binding energies) and the signal of the surface In atoms. Interestingly, the highly coordinated indium atoms of site B give the most positive CLS on the methanol-covered surfaces, whereas on the pristine surface, they exhibit mildly negative CLS with respect to the bulk indium atoms in the middle of the slab.

Additionally, we studied the adsorption of formic acid on stoichiometric $\text{In}_2\text{O}_3(111)$. The DFT calculations show that three formic acid molecules can adsorb dissociatively as a HCOO and H (with Bader charges of -0.75 and +0.64, respectively) pair around the B site, with the HCOO fragment in a bridging configuration between two In cations similar to the methoxy

groups. The next three HCOOH molecules adsorb dissociatively around the C site: one oxygen of the HCOO fragment binds to an In cation, and the other coordinating to the H (see Figure 6 in the SI). Similarly to the case of methanol and water, adsorption around the C site is less favourable than around the B site. In contrast, the adsorption of HCOOH at site C is, however, exothermic relative to the gas phase. This indicates that $\text{In}_2\text{O}_3(111)$ can accommodate six formic acid molecules per unit cell.

The experimental XPS spectra are displayed in Figure 4. The O 1s spectrum shows an additional peak at 532.6 eV with a large FWHM of 1.5 eV indicating that multiple components are contributing to this peak. After the adsorption of formic acid, the In $3d_{5/2}$ shows an increased asymmetry, similar to the methanol case. The C 1s spectrum shows a peak at 289.3 eV.

The computed O 1s CLS for HCOOH on the surface shows three groups of peaks. The surface oxygens that do not take part in the HCOOH adsorption show the lowest relative shifts. The O_sH groups around site C have an average shift of 1.4 eV, whereas HCOO and O_sH groups around site B have shifts ranging from 1.8 to 2.2 eV. The computed O 1s shifts are in fair agreement with the O 1s XPS spectrum. Similarly to methanol adsorption, the In 3d CLS show that the surface In cations are shifted to slightly higher binding energies than on the pristine surface.

The C 1s CLS of the HCOOH were computed relative to the C 1s CLS of the reference O- CH_3 group (see SI for a detailed discussion). The calculations were performed by placing a dissociated methanol molecule in the same unit cell with formic acid, and calculating the total energy with a core hole on each carbon atom. The CLS were calculated for two separate cases, where the HCOO and H pair is bound to either the B site or the C site. The HCOO-fragment at the B site has a shift of 2.78 eV, while the HCOO bound to the C site has a shift of 2.82 eV, relative to O- CH_3 . The average relative CLS of the two HCOO-groups and the O- CH_3 group is close (2.8 eV) to the experimentally observed difference in the binding energy (2.6 eV) of the HCOOH and O- CH_3 C 1s peaks. Further analysis on the effect of

the binding configuration, exchange-correlation functional, initial and final state effects, and surface coverage on calculated C 1s core-level shifts is presented in the SI.

The number of formic acid molecules per unit cell can be estimated from the area of the C 1s peak using the peak intensity of the O-CH₃-peak as a reference, under the assumption that this saturated surface is covered by three dissociated methoxy-molecules. Based on this assumption and the support from the DFT calculated adsorption energy trends, we can conclude that six formic acid molecules can adsorb per unit cell, as illustrated in Figure 3(b).

CO₂ adsorption on different surface terminations of In₂O₃(111)

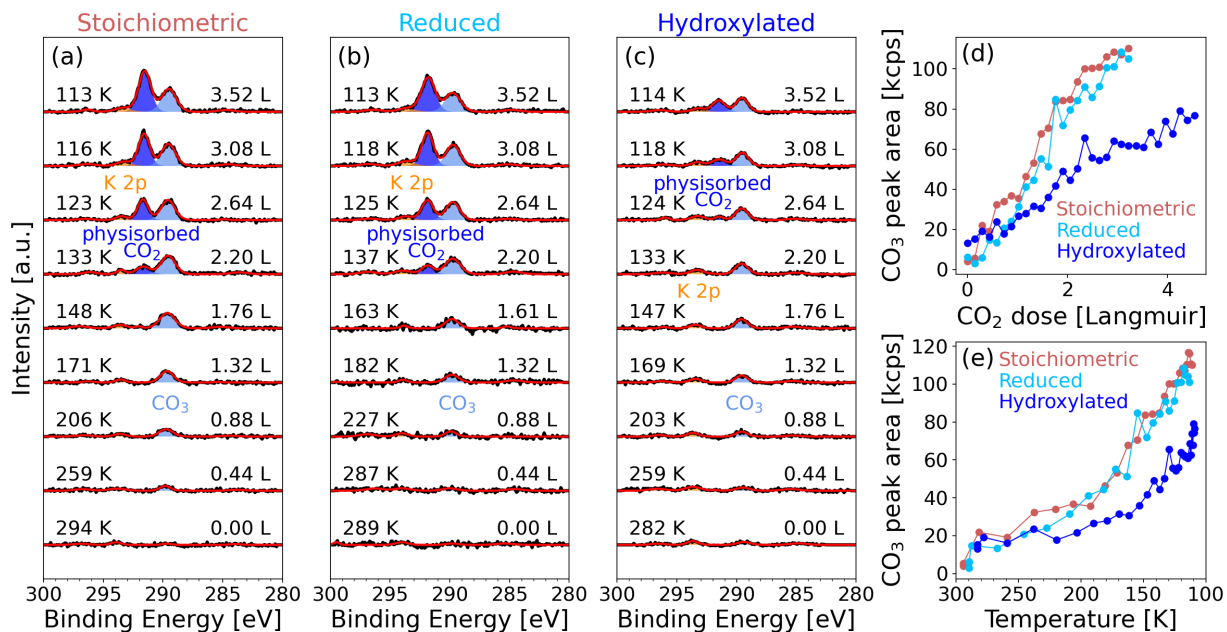


Figure 5: Measurements of CO₂ adsorption during sample cooling. C 1s core-level of (a) the stoichiometric surface, (b) the reduced surface and (c) the hydroxylated surface during CO₂ adsorption at mbar CO₂ while the samples are cooled down from room temperature to 100 K. The numbers on the left hand side of every panel give the temperature in Kelvin as the samples are cooled down and the numbers on the right hand side of the panel gives the CO₂ dose in Langmuir. Panel (d) shows the area of the CO₃ peak as a function of CO₂ dose in Langmuir and panel (e) shows the CO₃ peak area as a function of the sample temperature.

The adsorption of CO₂ was monitored experimentally on different terminations of the

In₂O₃(111) surface. The surfaces were exposed to 5×10^{-9} mbar CO₂ while being cooled from room temperature to 100 K. We chose this experimental route to minimize the adsorption of H₂O from the background that would otherwise occur when first cooling the sample and later dosing CO₂. Figure 5(a), 5(b) and 5(c) show the C 1s spectra of the stoichiometric, the reduced and the hydroxylated In₂O₃(111) during CO₂ adsorption, respectively. On all three surfaces, CO₂ adsorption results in the development of an XPS feature at 289.6 ± 0.1 eV. Its position is consistent with the formation of carbonate (CO₃).⁴⁵ The peak becomes visible on all three surfaces at temperatures around 200 K and grows as the sample is cooled further. In comparison, the peak growth is slower on the hydroxylated surface than on the other two surface terminations, indicating that the hydroxyl groups on this surface hinder the adsorption of CO₂. Conversely, adsorption on the reduced surface proceeds in a similar way as on the stoichiometric surface, showing that In ad-atoms do not affect the CO₂ adsorption. Figures 5(d) and 5(e) show the peak area of the carbonate peak as a function of the amount of dosed CO₂ and temperature, respectively. A new peak appears as the surfaces are cooled down to 140 K. This peak has a binding energy of 291.6 ± 0.1 eV, which originates from physisorbed CO₂.⁴⁵ Again, the growth of this peak is considerably slower on the hydroxylated surface.

We performed DFT calculations to identify the adsorption configuration of CO₂ on the differently terminated In₂O₃(111) surfaces. The resulting structures are illustrated in Figure 6. On the pristine surface, the CO₂ molecule can only adsorb by binding to a surface oxygen as a bent carbonate (CO₃) species with a Bader charge of -1.46 e. The adsorption is preferred on the undercoordinated oxygen atoms around the B site (Figure 6a). Here, the adsorption energy is -0.9 eV. The adsorption energy is lowered when more than one CO₂ molecule is adsorbed at the B site, and once all three oxygen atoms are occupied, additional CO₂ adsorbs close to site A instead. The adsorption energy of additional CO₂ at site A is weak (-0.3 to -0.1 eV), which indicates that at most three CO₂ molecules can adsorb as carbonate on the pristine In₂O₃(111) surface. The C 1s CLS of the carbonate is 2.9 eV with

respect to the methoxy group peak. The relative shift is in good agreement with experiments as the difference in the binding energy of the methoxy and carbonate C 1s XPS peaks is 3.0 eV.

On the hydroxylated surface, the oxygen atoms close to site B have all been converted to hydroxyl groups. The OH_{ads} and O_sH pair bind stronger to the site than CO_2 , and preferably occupy adjacent sites.¹⁹ It is energetically unfavorable to displace a hydroxyl group and to form a carbonate, thus CO_2 adsorption is blocked by water at the B site. The only sites left available for CO_2 adsorption are the oxygen atoms around site A, where the adsorption energy of a single CO_2 is -0.7 eV. Adsorption of additional CO_2 is less favorable: -0.5 and -0.4 eV for the second and third molecule, respectively. Interestingly, adsorption of carbonate at site A is more favorable when site B hosts water than when it hosts other carbonate species. Unlike dissociated water, the formation of a carbonate requires a charge transfer from the surface to adsorbate, thus the $\text{In}_2\text{O}_3(111)$ is not able to accommodate as many carbonates.

As an alternative to adsorbing as carbonate, CO_2 could in principle react with one of the O_sH or OH_{ads} groups on the hydroxylated surface to form formate (HCOO^-) or bicarbonate (HCO_3^-). The carbon atom of the formate species has a C 1s CLS of 3.0 eV with respect to the methoxy group peak (similar to the value of 2.9 eV of C 1s of carbonate species, see above), which would also be in very good agreement with the XPS data. However, adsorption is highly endothermic (approximately 3 eV) and thus unfavorable. Bicarbonate species are more stable than formate, however, the calculated C 1s CLS of all considered HCO_3^- -configurations are strongly shifted, approximately 4 eV higher binding energy, with respect to the methoxy peak. Therefore, we propose that CO_2 adsorbs as a carbonate also on the hydroxylated surface.

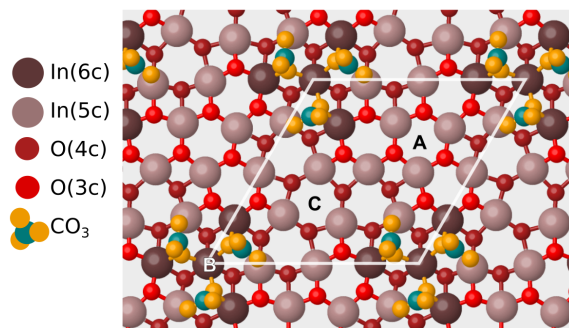
On reduced $\text{In}_2\text{O}_3(111)$, we find that CO_2 can adsorb as a carbonate in essentially the same geometry as on the pristine surface, additionally coordinating to the In ad-atom. A single carbonate pushes the ad-atom off-center of the B site so that it preferably occupies the

two-fold coordinate site, however, addition of more CO_2 pushes the ad-atom to the central position. The carbonate adsorption energy is more exothermic than on the pristine surface, and it is possible to populate all three B-site oxygen atoms simultaneously.

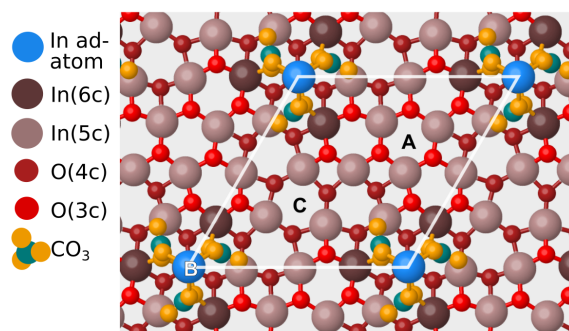
It is possible to estimate the number of molecules per unit cell by comparing the peak area of the adsorbed CO_3 in the experimental C 1s spectrum to the peak area of the adsorbed methanol. With a methanol coverage of three molecules per unit cell, the CO_2 coverage on the stoichiometric and reduced surface corresponds to approximately 1.7 molecules per unit cell, and to one molecule per unit cell on the hydroxylated surface. While the experimentally observed coverage on the hydroxylated surface is in agreement with the DFT calculations, the experimental coverage on the stoichiometric and on the reduced surface of 1.7 molecules per unit cell is lower than the three molecules per unit cell predicted by DFT calculations. We speculate that the discrepancy is due to the adsorption of water from residual gas in the vacuum chamber as the samples are cooled down. The adsorbed water molecules effectively block adsorption sites for the CO_2 as they do on the hydroxylated surface and thus lower the CO_2 coverage observed in the experiments.

Figures 7 and 8 show the experimental XPS spectra of the O 1s and the In $3d_{5/2}$ core-level of the three surface terminations after CO_2 adsorption, respectively. To support the experimental data, we also performed DFT calculations for CO_2 adsorbed in a carbonate configuration on the three $\text{In}_2\text{O}_3(111)$ surface terminations. The CLS in Figures 7 and 8 were calculated at a coverage of three carbonates per unit cell for the pristine and reduced surface, and one carbonate per unit cell for the hydroxylated surface. For the stoichiometric $\text{In}_2\text{O}_3(111)$, a minor broadening of the In_2O_3 peak in the O 1s and In 3d core-level is observed after the CO_2 adsorption. The adsorption of CO_2 appears to diminish the peak from the In ad-atoms by 55 % in the In 3d core-level whereas no change is observed in the O 1s spectrum. For the hydroxylated surface, the O 1s peak and the In 3d peak broaden after CO_2 adsorption. The DFT calculations show that the oxygen atoms of the carbonate (CO_3) are positively shifted with respect to a bulk oxygen on the pristine surface, however the

(a) CO₂ on stoichiometric In₂O₃(111)



(b) CO₂ on reduced In₂O₃(111)



(c) CO₂ on hydroxylated In₂O₃(111)

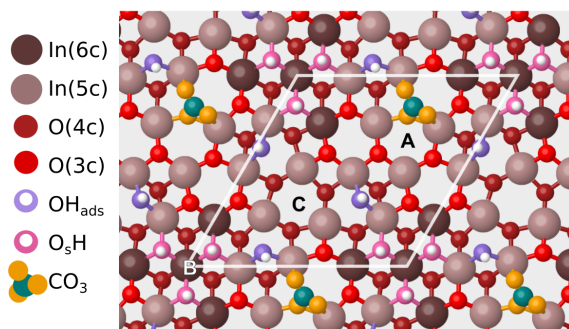


Figure 6: DFT-relaxed structures of CO₂ adsorption on (a) stoichiometric In₂O₃(111), (b) reduced In₂O₃(111) and (c) hydroxylated In₂O₃(111). Carbon atoms are colored teal, while the oxygen atoms forming the CO₃ carbonate species are colored orange.

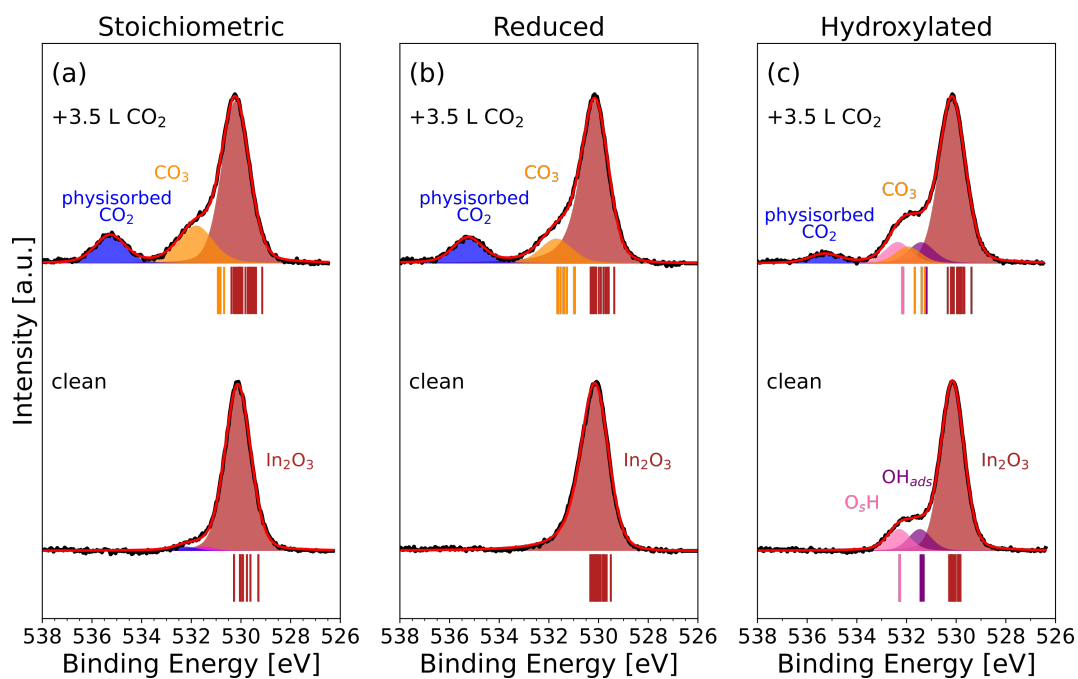


Figure 7: O 1s core-level spectra of (a) the stoichiometric, (b) the reduced and (c) the hydroxylated $\text{In}_2\text{O}_3(111)$ surface at room temperature prior to the adsorption of CO_2 (bottom), and after the adsorption of 3.5 L CO_2 at $5 \cdot 10^{-9}$ mbar (top) at the final temperature of approximately 100 K. The corresponding calculated CLS are indicated with vertical lines under each spectrum, their colors match the coloring of the atoms in the atomic structure figures.

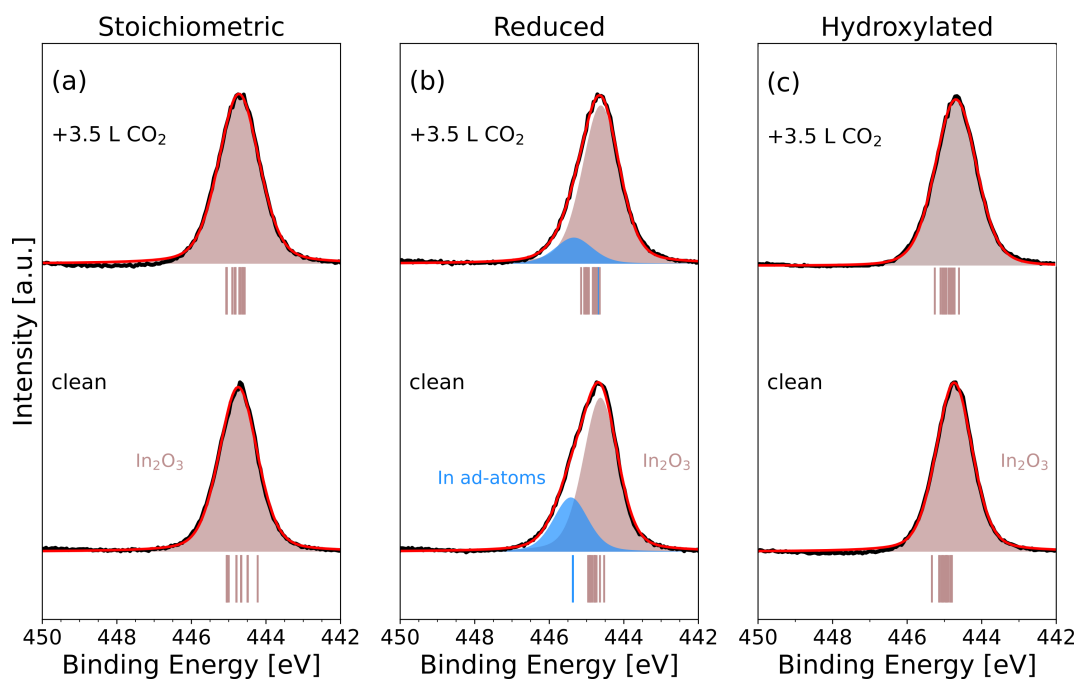


Figure 8: In 3d_{5/2} core-level spectra of (a) the stoichiometric, (b) the reduced and (c) the hydroxylated In₂O₃(111) surface at room temperature prior to the adsorption of CO₂ (bottom), and after the adsorption of 3.5 L CO₂ at 5 × 10⁻⁹ mbar (top) at the final temperature of approximately 100 K. The corresponding calculated CLS are indicated with vertical lines under each spectrum.

shifts are not as clearly distinguishable from the main surface oxygen peak as determined experimentally. On the reduced surface, the O 1s CLS of the CO₃ species and the surface oxygens are more separated and agree well with the experimental spectrum. Finally, on the hydroxylated surface, the CO₃ CLS are partially overlapping with the OH_{ads} peak, however the computed CLS are still in good qualitative agreement with the observed XPS. Calculated In 3d CLS show very little change upon CO₂ adsorption for the pristine and hydroxylated surface. On the reduced surface the CO₂ shifts the peak of the indium ad-atoms towards the bulk In₂O₃, agreeing very well with the experimentally observed suppression of the ad-atom peak upon CO₂ adsorption.

Discussion

We have presented XPS spectra of stoichiometric, reduced and hydroxylated In₂O₃(111), as well as changes upon adsorption of methanol and formic acid adsorbed on stoichiometric In₂O₃(111). The experimentally observed XPS spectra are overall in good agreement with the presented DFT core-level shift calculations. The experimental spectra and calculated CLS are important references for experiments performed at elevated pressures and temperatures.

Additionally, we studied the adsorption of CO₂ on different surface terminations of In₂O₃(111). The experiments showed that hydroxyl groups on In₂O₃(111) partially block the adsorption of CO₂. Water has been reported to decrease the activity of CO₂ hydrogenation for In₂O₃¹¹ and other CO₂ hydrogenation catalysts.⁴⁶ Our previous DFT-based microkinetic models have also shown that OH can block surface sites of In₂O₃(110), which leads to a negative reaction order with respect to the partial pressure of water.¹³ Our present DFT calculations indicate that water and CO₂ preferably adsorb at the same surface site. The dissociative water adsorption to the site is stronger than the physisorption of CO₂, therefore the resulting hydroxyl groups can block CO₂ from adsorbing as carbonate. Our computed C 1s core-level shift for carbonate closely matches the experimental shift rela-

tive to the methanol C 1s peak. The agreement between experiment and computations was achieved by using the well defined methanol and formic acid C 1s peaks as reference. For the C 1s CLS we find that including exact exchange by employing a hybrid functional is vital to achieve the correct relative shifts for carbon-containing adsorbates on $\text{In}_2\text{O}_3(111)$.

The adsorption of CO_2 on different catalysts for CO_2 hydrogenation such as CeO_2 , Rh and CuZn has been studied previously. CO_2 has been reported to adsorb as a carbonate on CeO_2 as well as on Zn deposited on copper surfaces,^{45,47} while it was reported to dissociate on Rh⁴⁸ and stepped Cu surfaces.⁴⁹ The present measurements show that CO_2 does not dissociate on $\text{In}_2\text{O}_3(111)$ when adsorbed at a pressure of 5×10^{-9} mbar and temperatures below room temperature. We could not observe the formation of formate on the surface when the CO_2 was adsorbed on the hydroxylated surface. This suggests that higher pressures, temperatures or additional gases are required to activate the CO_2 for the hydrogenation reaction. Our previous DFT studies suggest that the In_2O_3 surface is partially hydrogenated under typical reaction conditions,¹⁴ with kinetic studies on hydrogenated $\text{In}_2\text{O}_3(110)$ ¹³ supporting the notion that a hydrogenated surface forms the active site for the methanol synthesis from CO_2 . In contrast to the hydrogenated surface, hydroxylation by water does not result in a change in oxidation state^{14,50} for the surface In atoms, and does not facilitate the activation of CO_2 .

A detailed understanding of the adsorption of CO_2 on In_2O_3 is an important step towards understanding the catalytic process of thermal CO_2 hydrogenation over In_2O_3 -catalysts on the atomic scale. In a previous study, the reaction mechanism of CO_2 hydrogenation has been attributed to the interaction of reactants with O-vacancies.¹⁷ However, we have no evidence of the existence of these defects in the processes that we have studied so far.

The catalytic activity of In_2O_3 and CuZn increases when CO is added to the CO_2 and H_2 gas mixture.¹¹ In this context, it is interesting to note that for CuZn catalysts it has been shown that the increased activity results from the removal of hydroxyl groups from the surface by the CO via the WGS reaction.⁵¹ We speculate that a similar mechanism

may occur for the In_2O_3 surfaces, explaining the promotional effect of adding CO to the CO_2 and H_2 gas feed. Without calculating barriers, we can evaluate the thermodynamic feasibility of the WGS reaction on $\text{In}_2\text{O}_3(111)$ by considering the reaction between CO and a surface hydroxyl (see Figure 9). It has been shown previously in the case of $m\text{-ZrO}_2(\bar{1}11)$ that CO and OH cannot directly form formate in a single elementary step, and instead react to form its structural isomer, carboxyl.⁵² Thus, we also consider the WGS to proceed through carboxyl, which consequently dissociates into CO_2 and a proton on the surface. Our thermodynamic analysis shows that the reaction is feasible on the $\text{In}_2\text{O}_3(111)$, therefore it may be possible that CO can remove OH groups through WGS.

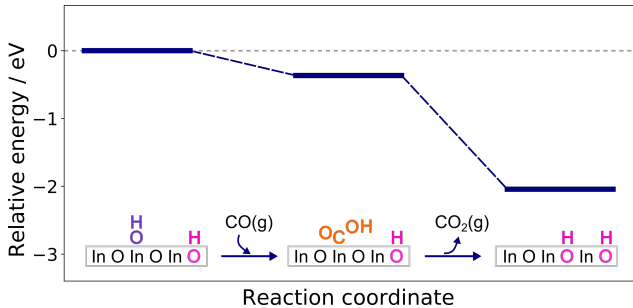


Figure 9: DFT calculated energy profile for the water-gas shift reaction between a surface $\text{O}_{\text{ads}}\text{H}$ group and a gas-phase CO.

Conclusions

We have studied different surface terminations of $\text{In}_2\text{O}_3(111)$, stoichiometric, reduced (with In ad-atoms), and hydroxylated, and the adsorption of CO_2 on these different surface terminations using XPS and DFT. Our results confirm the structure of the In ad-atom overlayer and the adsorption site of the hydroxyl groups reported in the literature. The experiments on the CO_2 adsorption showed that the In ad-atoms do not hinder the adsorption of CO_2 while hydroxyl groups on the surface partially block the adsorption of CO_2 . The DFT calculations showed that the CO_2 does not dissociate and adsorbs as a carbonate on all studied surface terminations of $\text{In}_2\text{O}_3(111)$.

Conflicts of interest

There are no conflicts to declare.

Acknowledgements

This project is financially supported by the Knut and Alice Wallenberg (KAW) project “Atomistic design of new catalysts” (project no. KAW2015.0058), the Swedish Research Council (project no. 2018-03434 and 2020-05191), the Swedish Foundation for Strategic Research (project no. ITM17-0045). The calculations were performed at PDC via a SNIC grant. This work was supported by the Austrian Science Fund (FWF), Project V 773-N (Elise-Richter-Stelle, M.W.). We acknowledge MAX IV Laboratory for time on Beamline FlexPES under Proposal 20200070 and 20210938. Research conducted at MAX IV, a Swedish national user facility, is supported by the Swedish Research council under contract 2018-07152, the Swedish Governmental Agency for Innovation Systems under contract 2018-04969, and Formas under contract 2019-02496. G.F. and U.D. acknowledge support from by the European Research Council (ERC) under the European Union’s Horizon 2020 research and innovation program (grant agreement No. 883395, Advanced Research Grant ‘WatFun’). M.R., A.I. and E.R. acknowledge support from the Austrian science fund (FWF) via the SFB project F81 “Taming complexity in materials modeling” (TACO).

Supporting Information

XPS Fits

Tables showing the line shapes, background shapes and FWHM of the XPS spectra shown in the main text.

DFT calculations

Comparison of stabilities, Bader charges, and In 3d core-level shifts of different ad-atom placements. Comparison of stabilities and PBE/HSE06-calculated C 1s core-level shifts of different carbon-containing species on the hydroxylated $\text{In}_2\text{O}_3(111)$ surface. Plots of adsorption energy as a function of coverage for water, methanol, formic acid, and CO_2 on the pristine $\text{In}_2\text{O}_3(111)$ surface. Plot of adsorption energies of CO_2 on the pristine, reduced and hydroxylated $\text{In}_2\text{O}_3(111)$ surface as a function of CO_2 (carbonate) coverage.

References

- (1) Zimov, S. A.; Schuur, E. A. G.; Chapin, F. S. Permafrost and the Global Carbon Budget. *Science* **2006**, *312*, 1612–1613.
- (2) Abelló, S.; Montané, D. Exploring iron-based multifunctional catalysts for fischer-tropsch synthesis: A review. *ChemSusChem* **2011**, *4*, 1538–1556.
- (3) Anderson, S.; Newell, R. Prospects for carbon capture and storage technologies. *Annu. Rev. Environ. Resour.* **2004**, *29*, 109–142.
- (4) Ye, R. P.; Ding, J.; Gong, W.; Argyle, M. D.; Zhong, Q.; Wang, Y.; Russell, C. K.; Xu, Z.; Russell, A. G.; Li, Q.; Fan, M.; Yao, Y. G. CO_2 hydrogenation to high-value products via heterogeneous catalysis. *Nat. Commun.* **2019**, *10*, 5698.
- (5) Zhang, X.; Zhang, G.; Song, C.; Guo, X. Catalytic Conversion of Carbon Dioxide to Methanol: Current Status and Future Perspective. *Frontiers in Energy Research* **2021**, *8*, 1–16.
- (6) Wang, S.; Wu, Z.; Xu, C.; Jiang, S.; Peng, H. Q.; Zhang, W.; Liu, B.; Song, Y. F. Triple-Phase Interface Engineering over an In_2O_3 Electrode to Boost Carbon Dioxide Electroreduction. *ACS Applied Materials and Interfaces* **2022**, *14*, 45423–45432.

- (7) Pan, B.; Yuan, G.; Zhao, X.; Han, N.; Huang, Y.; Feng, K.; Cheng, C.; Zhong, J.; Zhang, L.; Wang, Y.; Li, Y. Highly Dispersed Indium Oxide Nanoparticles Supported on Carbon Nanorods Enabling Efficient Electrochemical CO₂ Reduction . *Small Science* **2021**, *1*, 2100029.
- (8) Ganji, P.; Chowdari, R. K.; Likozar, B. Photocatalytic Reduction of Carbon Dioxide to Methanol: Carbonaceous Materials, Kinetics, Industrial Feasibility, and Future Directions. *Energy and Fuels* **2023**,
- (9) Twigg, M. V.; Spencer, M. S. Deactivation of copper metal catalysts for methanol decomposition, methanol steam reforming and methanol synthesis. *Top. Catal.* **2003**, *22*, 191–203.
- (10) Liang, B.; Ma, J.; Su, X.; Yang, C.; Duan, H.; Zhou, H.; Deng, S.; Li, L.; Huang, Y. Investigation on Deactivation of Cu/ZnO/Al₂O₃ Catalyst for CO₂ Hydrogenation to Methanol. *Ind. Eng. Chem. Res.* **2019**, *58*, 9030–9037.
- (11) Martin, O.; Martín, A. J.; Mondelli, C.; Mitchell, S.; Segawa, T. F.; Hauert, R.; Drouilly, C.; Curulla-Ferré, D.; Pérez-Ramírez, J. Indium oxide as a superior catalyst for methanol synthesis by CO₂ hydrogenation. *Angew. Chem., Int. Ed. Engl.* **2016**, *55*, 6261–6265.
- (12) Wagner, M.; Seiler, S.; Meyer, B.; Boatner, L. A.; Schmid, M.; Diebold, U. Reducing the In₂O₃(111) Surface Results in Ordered Indium Adatoms. *Adv. Mater. Interfaces* **2014**, *1*, 1400289.
- (13) Posada-Borbón, A.; Grönbeck, H. A First-Principles-Based Microkinetic Study of CO₂ Reduction to CH₃OH over In₂O₃(110). *ACS Catal.* **2021**, *11*, 9996–10006.
- (14) Posada-Borbón, A.; Grönbeck, H. Hydrogen adsorption on In₂O₃(111) and In₂O₃(110). *Phys. Chem. Chem. Phys.* **2020**, *22*, 16193–16202.

- (15) Posada-Borbón, A.; Bosio, N.; Grönbeck, H. On the signatures of oxygen vacancies in O1s core level shifts. *Surf. Sci* **2021**, *705*, 121761.
- (16) Bielz, T.; Lorenz, H.; Amann, P.; Klötzer, B.; Penner, S. Water-gas shift and formaldehyde reforming activity determined by defect chemistry of polycrystalline In_2O_3 . *J. Phys. Chem. C* **2011**, *115*, 6622–6628.
- (17) Mechanism and microkinetics of methanol synthesis via CO_2 hydrogenation on indium oxide. *Journal of Catalysis* **2018**, *361*, 313–321.
- (18) Franceschi, G.; Wagner, M.; Hofinger, J.; Krajňák, T.; Schmid, M.; Diebold, U.; Riva, M. Growth of In_2O_3 (111) thin films with optimized surfaces. *PRMaterials* **2019**, *3*, 1–10.
- (19) Wagner, M.; Lackner, P.; Seiler, S.; Brunsch, A.; Bliem, R.; Gerhold, S.; Wang, Z.; Osiecki, J.; Schulte, K.; Boatner, L. A.; Schmid, M.; Meyer, B.; Diebold, U. Resolving the Structure of a Well-Ordered Hydroxyl Overlayer on $\text{In}_2\text{O}_3(111)$: Nanomanipulation and Theory. *ACS Nano* **2017**, *11*, 11531–11541.
- (20) Preobrajenski, A.; Generalov, A.; Öhrwall, G.; Tchapyguine, M.; Tarawneh, H.; Appelfeller, S.; Frampton, E.; Walsh, N. FlexPES: a versatile soft X-ray beamline at MAX IV Laboratory. *Journal of Synchrotron Radiation* **2023**, *30*, 831–840.
- (21) Zhang, Z.; Yates, J. T. Band bending in semiconductors: Chemical and physical consequences at surfaces and interfaces. 2012.
- (22) Fairley, N. *CasaXPS Manual 2.3. 15: Introduction to XPS and AES*; Casa Software, 2009.
- (23) Kresse, G.; Hafner, J. Ab initio molecular dynamics for liquid metals. *Phys. Rev. B* **1993**, *47*, 558–561.

- (24) Kresse, G.; Hafner, J. Ab initio molecular-dynamics simulation of the liquid-metalamorphous- semiconductor transition in germanium. *Phys. Rev. B* **1994**, *49*, 14251–14269.
- (25) Kresse, G.; Furthmüller, J. Efficiency of ab-initio total energy calculations for metals and semiconductors using a plane-wave basis set. *Comput. Mater. Sci.* **1996**, *6*, 15–50.
- (26) Kresse, G.; Furthmüller, J. Efficient iterative schemes for ab initio total-energy calculations using a plane-wave basis set. *Phys. Rev. B* **1996**, *54*, 169.
- (27) Perdew, J. P.; Burke, K.; Ernzerhof, M. Generalized Gradient Approximation Made Simple. *PRL* **1996**, *77*, 3865–3868.
- (28) Perdew, J. P.; Burke, K.; Ernzerhof, M. Erratum: Generalized Gradient Approximation Made Simple. *PRL* **1997**, *78*, 1396.
- (29) Heyd, J.; Scuseria, G. E.; Ernzerhof, M. Hybrid functionals based on a screened Coulomb potential. *J. Chem. Phys.* **2003**, *118*, 8207–8215.
- (30) Heyd, J.; Scuseria, G. E.; Ernzerhof, M. Erratum: "Hybrid functionals based on a screened Coulomb potential" [J. Chem. Phys. 118, 8207 (2003)]. *J. Chem. Phys.* **2006**, *124*, 219906.
- (31) Krukau, A. V.; Vydrov, O. A.; Izmaylov, A. F.; Scuseria, G. E. Influence of the exchange screening parameter on the performance of screened hybrid functionals. *J. Chem. Phys.* **2006**, *125*, 224106.
- (32) Kresse, G.; Joubert, D. From ultrasoft pseudopotentials to the projector augmented-wave method. *Phys. Rev. B* **1999**, *59*, 1758–1775.
- (33) Pehlke, E.; Scheffler, M. Evidence for site-sensitive screening of core holes at the Si and Ge(001) surface. *Phys. Rev. Lett.* **1993**, *71*, 2338–2341.

- (34) Mårtensson, N.; Nilsson, A. On the origin of core-level binding energy shifts. *JESRP* **1995**, *75*, 209–223.
- (35) Grönbeck, H.; Klacar, S.; Martin, N. M.; Hellman, A.; Lundgren, E.; Andersen, J. N. Mechanism for reversed photoemission core-level shifts of oxidized Ag. *Phys. Rev. B* **2012**, *85*, 115445.
- (36) Delesma, F. A.; Van den Bossche, M.; Grönbeck, H.; Calaminici, P.; Köster, A. M.; Pettersson, L. G. M. A Chemical View on X-ray Photoelectron Spectroscopy: the ESCA Molecule and Surface-to-Bulk XPS Shifts. *ChemPhysChem* **2018**, *19*, 169–174.
- (37) Van den Bossche, M.; Martin, N. M.; Gustafson, J.; Hakanoglu, C.; Weaver, J. F.; Lundgren, E.; Grönbeck, H. Effects of non-local exchange on core level shifts for gas-phase and adsorbed molecules. *J. Chem. Phys.* **2014**, *141*, 034706.
- (38) Tang, W.; Sanville, E.; Henkelman, G. A Grid-Based Bader Analysis Algorithm Without Lattice Bias. *J. Phys. Condens. Mat.* **2009**, *21*, 084204.
- (39) Henkelman, G.; Arnaldsson, A.; Jónsson, H. A Fast and Robust Algorithm for Bader Decomposition of Charge Density. *Comp. Mater. Sci.* **2006**, *36*, 354–360.
- (40) Yu, M.; Trinkle, D. R. Accurate and Efficient Algorithm for Bader Charge Integration. *J. of Chem. Phys.* **2011**, *134*, 064111.
- (41) Sanville, E.; Kenny, S. D.; Smith, R.; Henkelman, G. Improved Grid-Based Algorithm for Bader Charge Allocation. *J. Comput. Chem.* **2007**, *28*, 899–908.
- (42) Hagleitner, D. R.; Menhart, M.; Jacobson, P.; Blomberg, S.; Schulte, K.; Lundgren, E.; Kubicek, M.; Fleig, J.; Kubel, F.; Puls, C.; Limbeck, A.; Hutter, H.; Boatner, L. A.; Schmid, M.; Diebold, U. Bulk and surface characterization of In₂O₃(001) single crystals. *Phys. Rev. B Condens. Matter Mater* **2012**, *85*, 1–11.

- (43) King, P. D.; Veal, T. D.; Fuchs, F.; Wang, C. Y.; Payne, D. J.; Bourlange, A.; Zhang, H.; Bell, G. R.; Cimalla, V.; Ambacher, O.; Egdell, R. G.; Bechstedt, F.; McConville, C. F. Band gap, electronic structure, and surface electron accumulation of cubic and rhombohedral In_2O_3 . *Phys. Rev. B Condens. Matter Mater* **2009**, *79*, 1–10.
- (44) Chen, H.; Blatnik, M. A.; Ritterhoff, C. L.; Sokolović, I.; Mirabella, F.; Franceschi, G.; Riva, M.; Schmid, M.; Čechal, J.; Meyer, B.; Diebold, U.; Wagner, M. Water Structures Reveal Local Hydrophobicity on the $\text{In}_2\text{O}_3(111)$ Surface. *ACS Nano* **2022**, *3*, 21163–21173.
- (45) Yang, C.; Bebensee, F.; Chen, J.; Yu, X.; Nefedov, A.; Wöll, C. Carbon Dioxide Adsorption on $\text{CeO}_2(110)$: An XPS and NEXAFS Study. *ChemPhysChem* **2017**, *18*, 1874–1880.
- (46) Saito, M.; Fujitani, T.; Takeuchi, M.; Watanabe, T. Development of copper/zinc oxide-based multicomponent catalysts for methanol synthesis from carbon dioxide and hydrogen. *APPL CATAL A-GE* **1996**, *138*, 311–318.
- (47) Koitaya, T.; Yamamoto, S.; Shiozawa, Y.; Yoshikura, Y.; Hasegawa, M.; Tang, J.; Takeuchi, K.; Mukai, K.; Yoshimoto, S.; Matsuda, I.; Yoshinobu, J. CO_2 Activation and Reaction on Zn-Deposited Cu Surfaces Studied by Ambient-Pressure X-ray Photoelectron Spectroscopy. *ACS Catal.* **2019**, *9*, 4539–4550.
- (48) Kim, J.; Ha, H.; Doh, W. H.; Ueda, K.; Mase, K.; Kondoh, H.; Mun, B. S.; Kim, H. Y.; Park, J. Y. How Rh surface breaks CO_2 molecules under ambient pressure. *Nat. Commun.* **2020**, *11*, 5649.
- (49) Hagman, B.; Posada-Borbón, A.; Schaefer, A.; Shipilin, M.; Zhang, C.; Merte, L. R.; Hellman, A.; Lundgren, E.; Grönbeck, H.; Gustafson, J. Steps Control the Dissociation of CO_2 on $\text{Cu}(100)$. *J. Am. Chem. Soc.* **2018**, *140*, 12974–12979.

- (50) Posada-Borbón, A.; Grönbeck, H. CO₂ adsorption on hydroxylated In₂O₃(110). *Phys. Chem. Chem. Phys.* **2019**, *21*, 21698–21708.
- (51) Ruland, H.; Song, H.; Laudenschleger, D.; Stürmer, S.; Schmidt, S.; He, J.; Kähler, K.; Muhler, M.; Schlögl, R. CO₂ Hydrogenation with Cu/ZnO/Al₂O₃: A Benchmark Study. *ChemCatChem* **2020**, *12*, 3216–3222.
- (52) Kauppinen, M. M.; Melander, M. M.; Bazhenov, A. S.; Honkala, K. Unraveling the Role of the Rh-ZrO₂ Interface in the Water-Gas-Shift Reaction via a First-Principles Microkinetic Study. *ACS Catal.* **2018**, *8*, 11633–11647.

stoichiometric $\text{In}_2\text{O}_3(111)$ hydroxylated $\text{In}_2\text{O}_3(111)$

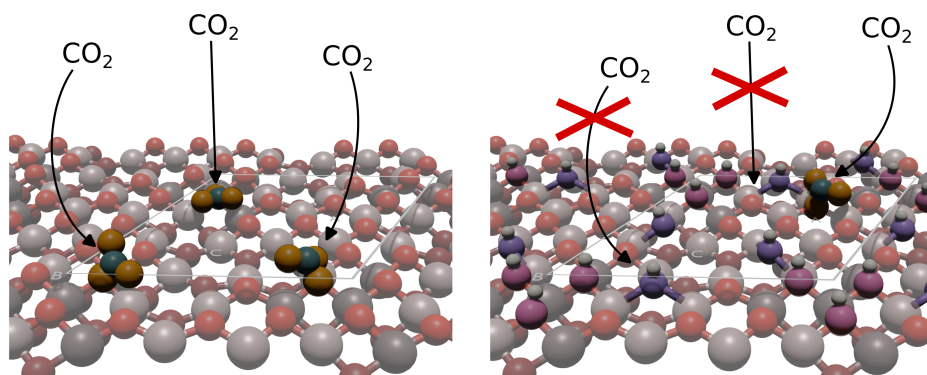


Figure 10: Table Of Contents (TOC) graphic.

Supplementary Information: The effect of different $\text{In}_2\text{O}_3(111)$ surface terminations on CO_2 adsorption

Sabrina M. Gericke,^{*,†,ⓐ} Minttu M. Kauppinen,^{*,†,ⓐ} Margareta Wagner,[¶]
Michele Riva,[¶] Giada Franceschi,[¶] Alvaro Posada-Borbón,[‡] Lisa Rämisch,[†]
Sebastian Pfaff,[†] Erik Rheinfrank,[¶] Alexander M. Imre,[¶] Alexei B.
Preobrajenski,[§] Stephan Appelfeller,[§] Sara Blomberg,^{||} Lindsay R. Merte,[⊥]
Johan Zetterberg,[†] Ulrike Diebold,[¶] Henrik Grönbeck,[‡] and Edvin Lundgren[#]

[†]*Division of Combustion Physics, Lund University, 221 00 Lund, Sweden.*

[‡]*Department of Physics and Competence Centre for Catalysis, Chalmers University of
Technology, 412 96 Göteborg, Sweden.*

[¶]*Institute of Applied Physics, TU Wien, 1040 Vienna, Austria.*

[§]*MAX IV Laboratory, Lund University, 221 00 Lund, Sweden.*

^{||}*Department of Chemical Engineering, Lund University, 221 00 Lund, Sweden.*

[⊥]*Department of Materials Science and Applied Mathematics, Malmö University, 205 06
Malmö, Sweden.*

[#]*Division of Synchrotron Radiation Research, Lund University, 221 00 Lund, Sweden.*

[ⓐ]*Contributed equally to this work*

E-mail: sabrina_maria.gericke@forbrf.lth.se; minttu.m.kauppinen@jyu.fi

XPS fitting parameters

The following section contains the fitting parameters used for the XPS spectra in the main text.

Table S1: Fitting parameters for the XPS spectra in Figure 2 of the main text.

Surface termination	Core level	Peak label	Binding energy [eV]	FWHM [eV]	Line shape	Background shape
hydroxylated	In 3d _{5/2}	In ₂ O ₃	444.7	1.2	SGL(30)	Shirley
	O 1s	In ₂ O ₃	530.1	1.1	SGL(20)	Linear
	O 1s	OH _{ads}	531.4	1.1	SGL(20)	Linear
	O 1s	O _s H	532.3	1.1	SGL(20)	Linear
reduced	In 3d _{5/2}	In ₂ O ₃	444.6	1.1	SGL(30)	Shirley
	In 3d _{5/2}	In ad-atoms	445.4	1.1	SGL(30)	Shirley
	O 1s	In ₂ O ₃	530.2	1.2	LA(1,1.9,200)	Linear
stoichiometric	In 3d _{5/2}	In ₂ O ₃	444.7	1.2	SGL(30)	Shirley
	O 1s	In ₂ O ₃	530.2	1.2	SGL(20)	Linear
	O 1s	OH _{ads}	531.4	1.1	SGL(20)	Linear
	O 1s	O _s H	532.3	1.1	SGL(20)	Linear

Table S2: Fitting parameters for the O 1s spectra in Figure 4(a) of the main text.

Surface termination	Core level	Peak label	Binding energy [eV]	FWHM [eV]	Line shape	Background shape
stoichiometric	O 1s	In ₂ O ₃	530.2	1.2	SGL(20)	Linear
	O 1s	OH _{ads}	531.4	1.1	SGL(20)	Linear
	O 1s	O _s H	532.3	1.1	SGL(20)	Linear
methanol	O 1s	In ₂ O ₃	530.2	1.1	SGL(20)	Linear
	O 1s	O-CH ₃	531.2	1.3	SGL(20)	Linear
	O 1s	O _s H	532.3	1.3	SGL(20)	Linear
formic acid	O 1s	In ₂ O ₃	530.2	1.1	SGL(20)	Linear
	O 1s	HCOOH	532.6	1.5	SGL(20)	Linear

Table S3: Fitting parameters for the In 3d_{5/2} spectra in Figure 4(b) of the main text.

Surface termination	Core level	Peak label	Binding energy [eV]	FWHM [eV]	Line shape	Background shape
stoichiometric	In 3d _{5/2}	In ₂ O ₃	444.7	1.2	SGL(30)	Shirley
methanol	In 3d _{5/2}	In ₂ O ₃	444.8	1.1	LA(1,10,450)	Shirley
formic acid	In 3d _{5/2}	In ₂ O ₃	444.7	1.2	LA(1,3,450)	Shirley

Table S4: Fitting parameters for the C 1s spectra in Figure 4(c) of the main text.

Surface termination	Core level	Peak label	Binding energy [eV]	FWHM [eV]	Line shape	Background shape
methanol	C 1s	O-CH ₃	286.7	1.2	SGL(30)	Linear
formic acid	C 1s	HCOOH	289.3	1.0	SGL(30)	Linear

Table S5: Fitting parameters for the C 1s spectra in Figure 5(a), 5(b) and 5(c) of the main text.

Surface termination	Core level	Peak label	Binding energy [eV]	FWHM [eV]	Line shape	Background shape
stoichiometric	C 1s	physisorbed CO ₂	291.5	1.2	SGL(30)	Linear
	C 1s	CO ₃	289.5	1.3	SGL(30)	Linear
reduced	C 1s	physisorbed CO ₂	291.7	1.3	SGL(30)	Linear
	C 1s	CO ₃	289.7	1.4	SGL(30)	Linear
hydroxylated	C 1s	physisorbed CO ₂	291.5	1.2	SGL(30)	Linear
	C 1s	CO ₃	289.5	1.3	SGL(30)	Linear

Table S6: Fitting parameters for the O 1s spectra in Figure 7 of the main text for the spectra after CO₂ adsorption.

Surface termination	Core level	Peak label	Binding energy [eV]	FWHM [eV]	Line shape	Background shape
stoichiometric	O 1s	In ₂ O ₃	530.2	1.3	SGL(20)	Linear
	O 1s	CO ₃	531.8	1.1	SGL(20)	Linear
	O 1s	physisorbed CO ₂	535.3	1.1	SGL(20)	Linear
reduced	O 1s	In ₂ O ₃	530.2	1.3	SGL(20)	Linear
	O 1s	CO ₃	531.7	1.6	SGL(20)	Linear
	O 1s	physisorbed CO ₂	535.3	1.5	SGL(20)	Linear
hydroxylated	O 1s	In ₂ O ₃	530.2	1.3	SGL(20)	Linear
	O 1s	OH _{ads}	531.4	1.3	SGL(20)	Linear
	O 1s	CO ₃	531.9	1.3	SGL(20)	Linear
	O 1s	O _s H	532.4	1.3	SGL(20)	Linear
	O 1s	physisorbed CO ₂	535.3	1.4	SGL(20)	Linear

Table S7: Fitting parameters for the XPS spectra in Figure 8 of the main text for the spectra after CO₂ adsorption.

Surface termination	Core level	Peak label	Binding energy [eV]	FWHM [eV]	Line shape	Background shape
hydroxylated	In 3d _{5/2}	In ₂ O ₃	444.7	1.3	LA(1.5,200)	Shirley
reduced	In 3d _{5/2}	In ₂ O ₃	444.6	1.1	SGL(30)	Shirley
	In 3d _{5/2}	In ad-atoms	445.3	1.1	SGL(30)	Shirley
stoichiometric	In 3d _{5/2}	In ₂ O ₃	444.7	1.3	SGL(30)	Shirley

LEED images

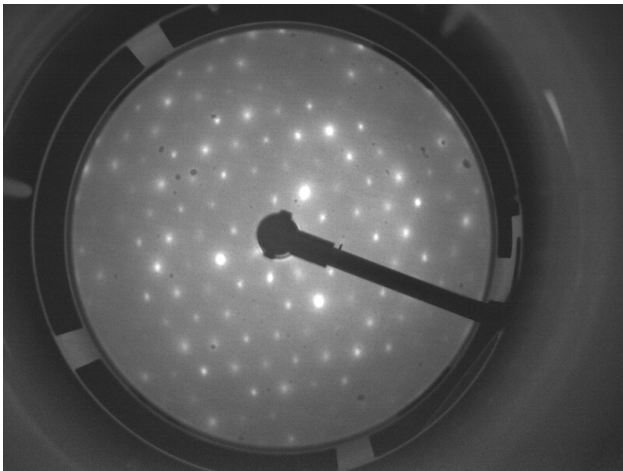


Figure S1: LEED image of the stoichiometric In₂O₃(111) surface measured with 63 eV.

Ad-atoms on reduced In₂O₃(111)

The relative stabilities and Bader charges of the In ad-atoms at different sites calculated at the PBE level of theory are given in Table S8. Geometries where the ad-atom binds to the A or C site are considerably higher in energy than at the B site.

The ad-atoms have In 3d core-level shifts (CLS) at higher binding energies with respect to the bulk indium atom (see Figure S3). Indeed, the ad-atoms should be shifted to higher binding energies compared to the bulk (and other low-coordinated surface indium atoms),

Table S8: Stabilities and Bader charges of In ad-atoms on different $\text{In}_2\text{O}_3(111)$ high symmetry sites. The stabilities are calculated with respect to B_h , the high-symmetry 3-fold hollow site created by O atoms at the B-site. B_b is a bridge site between two of the O atoms. The Bader charges at the different sites are obtained as the difference between the number of Bader electrons and electrons on the neutral atom of the element.

site	relative stability /eV	Bader charge
A	+0.83	+0.75
B_b	+0.00	+0.75
B_h	0	+0.77
C	+1.38	+0.74

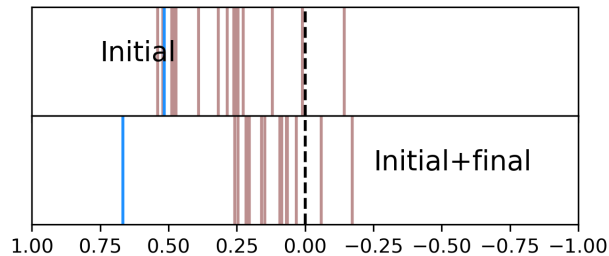


Figure S2: Surface In 3d core-level shifts for an ad-atom at B_b site of the $\text{In}_2\text{O}_3(111)$ surface calculated in the electrostatic initial state picture (top) and in the complete screening picture (bottom). The ad-atom CLS are shown in blue, while CLS from other surface In atoms are shown in brown. The dashed line shows the position of the bulk In.

due to the ad-atoms experiencing lower Madelung potentials compared to the bulk.^{S1,S2} However, final state effects arising from the electronic relaxation upon creating the core hole could still be important. To illustrate this, we obtained the In 3d CLS in the initial state picture by re-calculating the Kohn-Sham eigenvalues of the core states for the ad-atom bound at the B_b site. As can be seen in Fig. S2, the CLS for the ad-atom computed in the initial picture is not distinguishable from the other surface indium atoms. The inclusion of final state effects yields a larger positive shift for the ad-atom and less positive shifts for other surface indium atoms, allowing the shift from the ad-atom to be resolved.

The In 3d CLS of In atoms in the first O-In-O trilayer were calculated (including final state effects) for all ad-atom containing structures (Fig S3). All ad-atoms show a positive shift with respect to an In atom in the centre of the slab, shifted further than any other surface In atom.

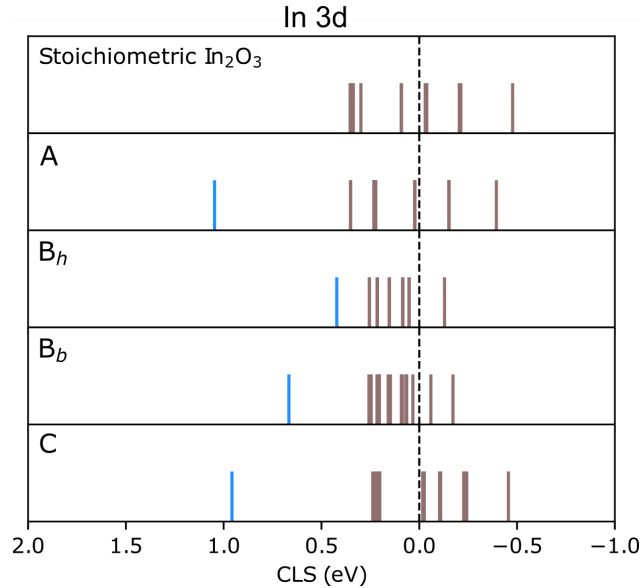


Figure S3: Surface In 3d CLS for stoichiometric and ad-atom containing $\text{In}_2\text{O}_3(111)$ surface. The ad-atom CLS are shown in blue, while CLS from other surface In atoms are shown in brown. The dashed line shows the position of the bulk In in each system.

Surface coverages of water, formic acid, and methanol

The effect of coverage on the adsorption energy of water, formic acid, and methanol were investigated on the stoichiometric $\text{In}_2\text{O}_3(111)$ in order to determine their saturation coverages. For each adsorbate, the most favourable adsorption sites were determined first for a single molecule in the unit cell. All three molecules prefer to adsorb at the B site dissociatively, formic acid having the strongest binding energy. The next best adsorption site for all molecules is around the C site, with water and methanol adsorbing molecularly to the site, while formic acid preferably donates a proton to a surface oxygen, binding in a tilted configuration. The structures with 1-3 molecules per unit cell were constructed by populating all three equivalent B sites one by one and relaxing the structures. Structures with 4-6 molecules per unit cell were constructed by taking the structure with all B sites occupied, adding molecules to site C one by one, and relaxing the obtained structures. The results

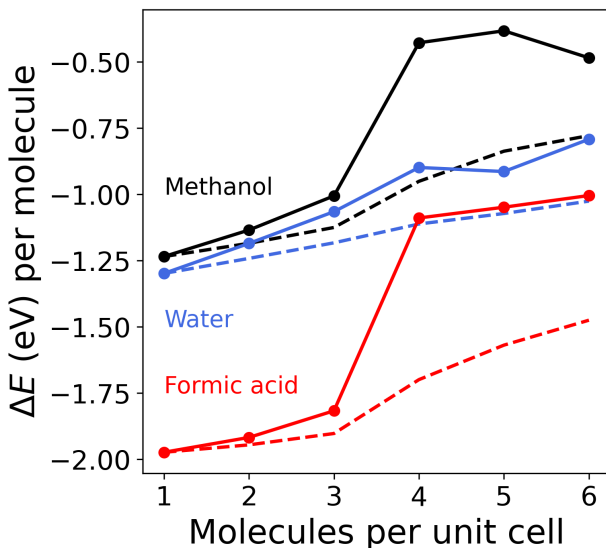


Figure S4: Differential (solid lines) and average (dashed lines) adsorption energies of water (blue), methanol (black), and formic acid (red) as a function of coverage.

(Fig. S4) show that the adsorption energy to the site B is only slightly lowered when more than one molecule is adsorbed around it. Differential adsorption energy to site C is much lower than site B, especially for formic acid and methanol, with increasing coverage having

only a small effect. Based on the adsorption energies, methanol and water should have a saturation coverage of 3 molecules per unit cell at room temperature. Formic acid adsorbs on the surface more strongly, and could achieve a saturation coverage of 6 molecules per unit cell.

Surface coverage of carbonate on stoichiometric, reduced, and hydroxylated $\text{In}_2\text{O}_3(111)$

Adsorption of CO_2 as a carbonate species was investigated on the stoichiometric, reduced, and hydroxylated terminations of $\text{In}_2\text{O}_3(111)$. On the stoichiometric surface, the CO_2 molecule binds to the oxygen atom around site B in a bent geometry. Incorporating three CO_2 molecules around the site is possible, with the differential adsorption energy decreasing upon addition of the second and third CO_2 .

On the reduced surface, the CO_2 can adsorb at the B-site oxygen atoms, coordinating also to the ad-atom which is adsorbed at the center of the B site. The adsorption of up to three CO_2 molecules around site B on the reduced $\text{In}_2\text{O}_3(111)$ is more exothermic than on the stoichiometric $\text{In}_2\text{O}_3(111)$, indicating that the presence of the ad-atom does not block adsorption of CO_2 as carbonate.

Effect of exact exchange and OH coverage on O 1s binding energies

The O 1s CLS of hydroxyl groups formed on $\text{In}_2\text{O}_3(111)$ upon dissociative water adsorption were calculated at the PBE and HSE06 level of theory with one (low coverage) and three (saturation coverage) dissociated water in the unit cell (Fig. S6). At low coverage, the PBE/HSE06 calculated O 1s CLS with respect to a bulk oxygen are 1.23/1.26 and 1.95/1.99 eV for the OH_{ads} and O_sH groups, respectively. At the saturation coverage, the OH_{ads} and

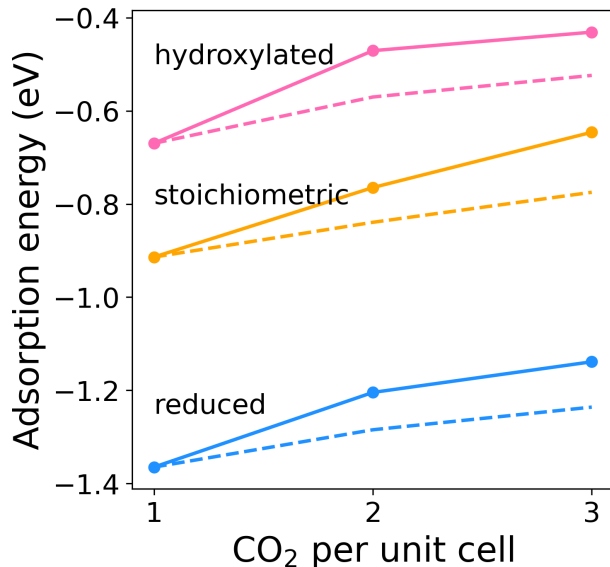


Figure S5: Differential (solid lines) and average (dashed lines) adsorption energies of carbonate as a function of coverage on stoichiometric (yellow), reduced (blue), and hydroxylated (pink) $\text{In}_2\text{O}_3(111)$.

O_sH groups give slightly different O 1s CLS, the average CLS computed using PBE/HSE06 being 1.28/1.40 and 2.17/2.30 eV, respectively. The PBE computed values at saturation coverage give the best agreement with experimental binding energy shifts (1.3 and 2.1 eV for OH_{ads} and O_sH , respectively). The PBE and HSE06 computed values at low coverage slightly underestimate the shifts with respect to experiments, especially for the O_sH species, while the HSE06 calculated values at saturation coverage slightly overestimate the shifts.

Carbon containing adsorbates on $\text{In}_2\text{O}_3(111)$

In order to support the peak assignment of the experimental XPS spectra of the CO_2 adsorption studies, the C 1s CLS of various possible adsorption structures (Fig. S7) have to be calculated. However, only relative CLS can be obtained within the applied methodology. Since there are no bulk carbon atoms in the stoichiometric In_2O_3 structure, there is no reference carbon atom in the system, unlike in the case of oxygen and indium. Therefore to provide a reference molecule on the surface that CLS of other adsorbates could be calculated

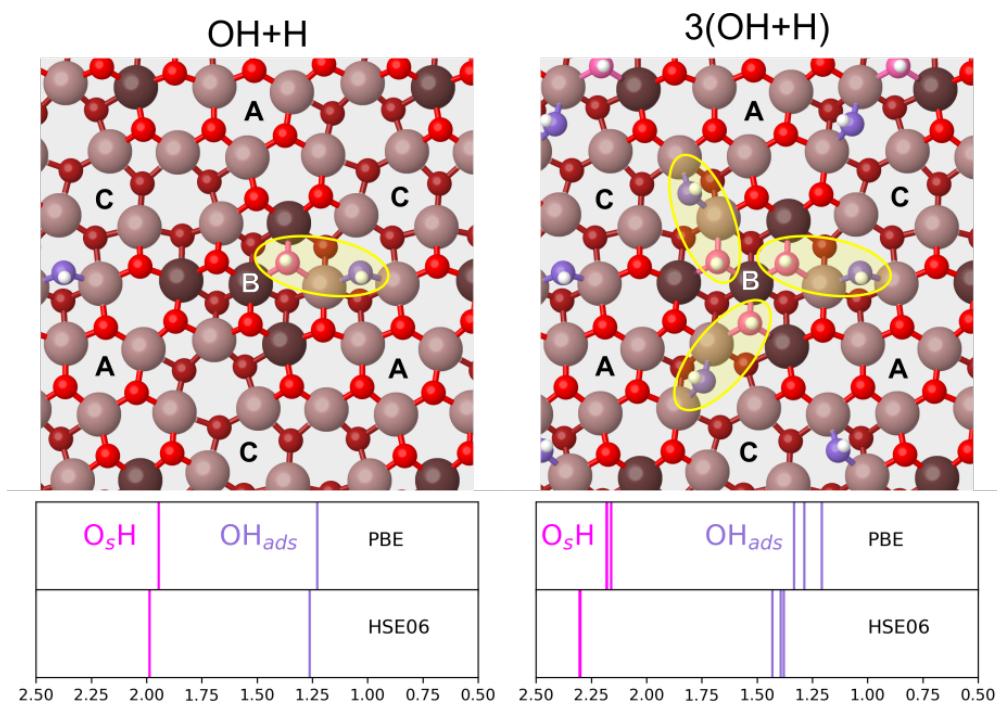


Figure S6: Optimised structures (top) and O 1s CLS (bottom) for hydroxyl group containing $\text{In}_2\text{O}_3(111)$ surfaces for two different coverages calculated with PBE and HSE06 functionals.

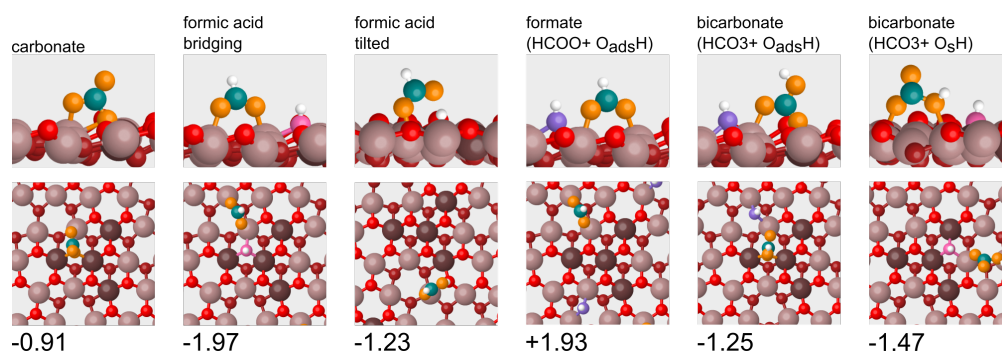


Figure S7: Optimised geometries and adsorption energies (in eV) of various carbon containing adsorbates on $\text{In}_2\text{O}_3(111)$. The adsorption energies are given with respect to the clean stoichiometric $\text{In}_2\text{O}_3(111)$ slab and CO_2 (carbonate), formic acid (formic acid), or CO_2 and H_2O (formate and bicarbonate) in the gas-phase.

with reference to, the adsorption of formic acid and methanol were studied experimentally on the stoichiometric $\text{In}_2\text{O}_3(111)$. Both molecules give clear peaks in the C 1s spectra, separated by 2.6 eV. To calculate the relative shift between formic acid and methanol, both molecules were placed on a stoichiometric $\text{In}_2\text{O}_3(111)$ slab in the same unit cell (Fig. S8). The relative C 1s core-level shift (ΔCLS), was then calculated with the gradient-corrected

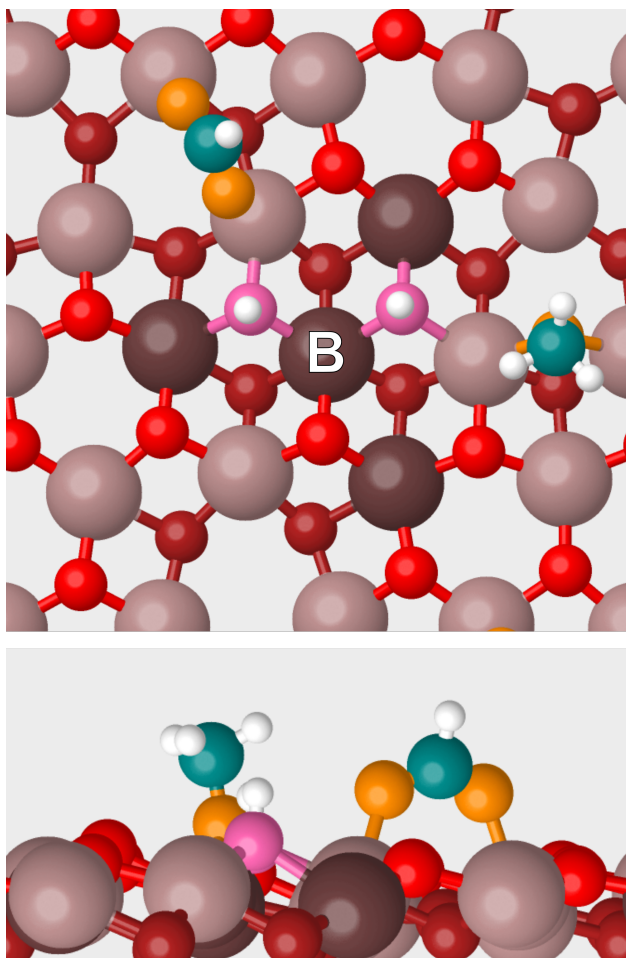


Figure S8: Formic acid and methanol adsorbed in the same $\text{In}_2\text{O}_3(111)$ unit cell for C 1s ΔCLS calculation.

PBE functional as a difference in the total energy of the system with the core hole either on the methanol or on the formic acid molecule. The calculated ΔCLS was 1.42 eV, clearly not in agreement with the experimental value of 2.6 eV. Previous calculations have shown that non-local exchange effects included in hybrid exchange-correlation functionals can lead to better agreement between the calculated CLS and experimental XPS data.^{S3,S4} To inves-

tigate this effect for CLS of $\text{In}_2\text{O}_3(111)$ surface species, the C 1s ΔCLS of various carbon containing adsorbates were calculated using PBE and HSE06 functionals, accompanied by Bader charge analysis. The C 1s ΔCLS and Bader charges are presented in table S9. The

Table S9: C 1s CLS (relative to methanol) and Bader charges (b.c.) on the carbon atom of carbon-containing adsorbates on stoichiometric $\text{In}_2\text{O}_3(111)$ calculated with PBE and HSE06.

Structure	ΔCLS (eV)			b.c. on C, adsorbate			b.c. on C, MeOH		
	PBE	HSE06	Δ	PBE	HSE06	Δ	PBE	HSE06	Δ
formic acid bridging	1.42	2.78	1.36	1.56	1.66	0.10	0.42	0.45	0.03
formic acid tilted	2.17	2.82	0.65	1.52	1.62	0.10	0.48	0.52	0.04
carbonate	2.42	2.92	0.50	2.05	2.22	0.17	0.46	0.49	0.03
formate ($\text{HCOO}+\text{O}_{\text{ads}}\text{H}$)	1.22	3.00	1.78	1.57	1.67	0.10	0.46	0.49	0.03
bicarbonate ($\text{HCO}_3+\text{O}_{\text{s}}\text{H}$)	3.27	3.91	0.64	2.08	2.22	0.14	0.47	0.49	0.02
bicarbonate ($\text{HCO}_3+\text{O}_{\text{ads}}\text{H}$)	3.82	4.65	0.83	2.18	2.29	0.11	0.43	0.46	0.03

HSE06 calculated C 1s ΔCLS for the formic acid is in much better agreement with the experimental value. In general, all carbon containing adsorbates studied here present more positively shifted C 1s ΔCLS when calculated with HSE06 as compared to PBE. This is consistent with the improved charge separation achieved with the HSE06 functional, the effect of which can be seen as more positive Bader charges on the adsorbate carbon atoms.

References

- (S1) Nelin, C. J.; Uhl, F.; Staemmler, V.; Bagus, P. S.; Fujimori, Y.; Sterrer, M.; Kuhlbeck, H.; Freund, H.-J. Surface core-level binding energy shifts for $\text{MgO}(100)$. *Phys. Chem. Chem. Phys.* **2014**, *16*, 21953–21956.
- (S2) Bagus, P. S.; Nelin, C. J.; Levchenko, S. V.; Zhao, X.; Davis, E. M.; Kuhlbeck, H.; Freund, H.-J. Surface core level BE shifts for $\text{CaO}(100)$: insights into physical origins. *Phys. Chem. Chem. Phys.* **2019**, *21*, 25431–25438.
- (S3) Van den Bossche, M.; Martin, N. M.; Gustafson, J.; Hakanoglu, C.; Weaver, J. F.;

Lundgren, E.; Grönbeck, H. Effects of non-local exchange on core level shifts for gas-phase and adsorbed molecules. *J. Chem. Phys.* **2014**, *141*, 034706.

(S4) Delesma, F. A.; Van den Bossche, M.; Grönbeck, H.; Calaminici, P.; Köster, A. M.; Pettersson, L. G. M. A Chemical View on X-ray Photoelectron Spectroscopy: the ESCA Molecule and Surface-to-Bulk XPS Shifts. *ChemPhysChem* **2018**, *19*, 169–174.